ENHANCING THE BIOCOMPATIBILITY OF 3D PRINTED Ti-6Al-4V ELI ALLOY WITH DIAMOND-LIKE CARBON (DLC) COATINGS

Jake Reneman

Bachelor of Engineering
Mechanical Engineering

Department of Engineering
Macquarie University

Supervisor: Dr Nicholas Tse

Commonwealth Scientific and Industrial Research Organisation (CSIRO)
Manufacturing
Lindfield, NSW

CSIRO Supervisors: Dr Avi Bendavid and Dr Samuel Yick

September 5, 2016

Acknowledgements

I would like to express my gratitude to all those involved in providing me with the opportunity and support required to complete this project. I give a special acknowledgement to Dr Avi Bendavid and Dr Samuel Yick who tirelessly offered their support, encouragement and expertise in assisting me to coordinate all aspects of this research project. I must also thank Dr Nicholas Tse for his role as my supervisor and mentor who provided me with his invaluable insight, assistance and guidance.

Furthermore, with much appreciation, I would like to acknowledge Dr Meg Evans and Miss Penny Bean for their vital roles with assisting me in devising the experimental methods and conducting the biological testing as presented in this research report. Additionally, I would like to thank Dr Darren Fraser for his role in providing me with the Electron Beam Melting (EBM) manufactured parts that we used for this project. Dr Phil Martin must also be acknowledged for assisting me with the LEIS measurements and for proof-reading my report.

Lastly, Macquarie University and CSIRO are acknowledged for the provision of funds and resources for this research project. This project would not have been possible without the guidance of aforementioned people.

Statement of Candidate

I, Jake Reneman, declare that this report, submitted as part of the requirement for the award of Bachelor of Engineering in the Department of Engineering, Macquarie University, is entirely my own work unless otherwise referenced or acknowledged. This document has not been submitted for qualification or assessment at any academic institution.

Student's Name: Jake Reneman

Student's Signature:

Date: November 7, 2016

Abstract

Orthopaedic implants are often required to restore normal functionality to the human body as a result of damage from illness, disease or injury. Ti-6Al-4V ELI is the current material of choice for orthopaedic surgeons as they are biocompatible and have excellent mechanical properties. Recent advancements in additive manufacturing (AM) techniques have allowed for the increased customisation of Ti-6Al-4V ELI implants to complement natural variations in the human anatomy. This can result in better patient outcomes and increase their post-operation quality of life. As biomedical implants need to be in the body long-term, it is vital to understand their biological interaction. Despite the prevalence of titanium alloy based implants, there are studies which indicate potential issues with regards to their osseointegration.

Diamond-like Carbon (DLC) is a thin film material which could be used to significantly enhance the longevity of an implant. DLC is an FDA approved material for biological applications. It has high wear resistance, corrosion resistance, high mechanical hardness and a low coefficient of friction. DLC coatings have been demonstrated to enhance *in vitro* osseointegration of cells in various studies.

We coated AM Ti-6Al-4V ELI with DLC to examine whether its biological properties can be improved. From the outcomes of our cell proliferation studies conducted using Saos-2 osteosarcoma cells, our DLC coatings significantly enhanced the rate of proliferation of cells as compared to the uncoated materials. Cell mineralisation studies also suggested that DLC coatings enhanced the calcium production of Saos-2 cells as compared to the uncoated materials, indicating that the cells on DLC materials were at a more advanced state of differentiation.

Table of Contents

List of Figures

List of Tables

1. Introduction

With Australia's ageing population, the need for medical procedures such as arthroplasty is becoming more prevalent. Orthopaedic implants are often required to restore normal functionality to the human body as a result of damage from illness, disease or injury. Currently, the major concern for the long-term survival of hip and knee implants is the degradation of polyethene debris which causes pain and premature aseptic loosening of the prosthesis [1]. The formation of this wear debris is the result of the high wear rates of the polyethene material when in cyclic contact with metals. A potential solution for this issue is the application of thin film coating technologies to improve all surfaces in the prosthesis. Diamond-like Carbon (DLC) is a material which could be used to enhance the wear resistance of materials.

Present arthroplasty surgery requires surgeons to fit commercially available implants to each individual patient. These implants are mass-produced and often do not conform to the specific requirements and dimensions of each individual, increasing the risk of revision surgery. Complications commonly occur if the implant is incorrectly fitted due to natural variations in the human anatomy. The lack of specificity can result in joint instability and significant pain for the patient. Modern additive manufacturing techniques allow surgeons to develop and customise implants that are unique to each patient. This form of technology can significantly improve the outcomes for patients.

Currently, Ti-6Al-4V ELI alloy is the most commonly used implant material due to its excellent strength and oxidation resistance properties, however, the inert behaviour of the material means that the alloy does not react with human tissues. This can often result in lower rates of cell attachment and proliferation which increases the recovery time for patients and also increases the risk of revision surgery for patients. Ti-6Al-4V ELI alloy has a high coefficient of friction and has been shown to exhibit extreme wear when in contact with itself during cyclic operations [2].

Modern additive manufacturing techniques are predominately restricted to using Ti-6Al-4V alloy as the build material for biomedical applications. The biocompatibility of additive manufactured materials has often been assumed to be the same as cast or wrought materials, however, this is likely to not be the case due to the differences in the surface chemistry and morphology of these materials. Further in-depth studies of the biocompatibility and cytotoxicity of additive manufactured materials are required to confirm its long-term biocompatibility. Studies have suggested that the long-term use of Ti-6Al-4V ELI has raised concerns with the breakdown of wear debris and the release of aluminium and vanadium into the body which can lead to inflammatory reactions [3, 4]. The leaching of

aluminium is of significant concern as the accumulation of aluminium ions in the brain has been linked with possible long-term health issues such as Parkinson's and Alzheimer's disease [1, 5, 6].

The scope of this research is to investigate the application a thin film DLC coating to Ti-6Al-4V ELI alloy materials that have been manufactured by Electron Beam Melting (EBM) technology. DLC is a U.S. Food and Drug Administration (FDA) approved material for biological applications which has high wear resistance, mechanical hardness and a low coefficient of friction. DLC has been shown to possess excellent biocompatibility *in vitro,* which is advantageous to improving the quality of the implant. In typically hard wearing environments such as the knee joint, a DLC coating is a strong candidate to significantly increase the working lifetime of an implant.

1.1 Project Goals

The aim to achieve the following goals by the completion of the research project:

1. To validate our hypothesis that DLC coatings can be successfully applied to EBM manufactured Ti-6Al-4V ELI alloy materials.
2. To perform material characterisation of EBM manufactured Ti-6Al-4V ELI and DLC coated materials.
3. To perform biological testing of EBM manufactured Ti-6Al-4V ELI and DLC coated materials to determine whether or not DLC coatings can enhance the biocompatibility of the 3D printed materials.

1.2 Project Deliverables

The deliverables of this project are closely aligned to the aforementioned goals. The project deliverables are presented below:

1. Collated data and supporting results to validate the hypothesis of the project.
2. A final thesis report which outlines and presents the findings of this research project.

1.3 Preliminary Work

Preliminary findings in this report were conducted during a work placement with CSIRO over the 2015/2016 summer vacation. During this placement, an investigation into the effectiveness of doped DLC coatings for EBM manufactured Ti-6Al-4V ELI materials was conducted. This study included a preliminary cytotoxicity, cell proliferation and bacterial resistance analysis of doped DLC coated materials.

1.3.1 Indirect Cytotoxicity Assay

Indirect cytotoxicity testing was conducted to screen for the presence of any toxic compounds in the media collected from each sample after extraction. The protocols used for the cytotoxicity testing were based on ISO 10993-5 *Biological evaluation of medical devices – Part 5: Tests for in vitro cytotoxicity* consistent with International Standards Organization (ISO) standard procedures. Cell viability of an extract above 70 % is considered acceptable and deemed to be non-cytotoxic to cells.

Indirect cytotoxicity testing revealed that the neat extract of the control EBM manufactured Ti-6Al-4V ELI was mildly cytotoxic to the cells. The DLC coated materials also showed marginal cytotoxicity when neat but this may have been due to the instability of the surface allowing the EBM material underneath to affect results. Imaging of these wells showed reduced cell number but otherwise healthy cells suggesting that only proliferation rate may be affected.

2. Literature Review

2.1 Additive Manufacturing (3D Printing)

Additive manufacturing (AM) is a process of constructing an object from 3D computer-aided design (CAD) model data, through the addition of material in a layer upon layer method [7]. AM techniques significantly reduce the amount of waste material as compared to traditional manufacturing techniques such as casting. AM has a diverse range of applications in the aerospace, biomedical, construction and automotive industries.

The main process for additive manufacturing is as follows [8]:

1. Creation of a CAD model.
2. Conversion to Standard Tessellation Language (STL) file format.
3. Transfer to additive manufacturing (AM) machine and STL file manipulation.
4. Setup of machine and process parameters.
5. Manufacturing (3D printing) of build part.
6. Build part removal from the machine.
7. Post processing and removal of support structures from build part.

High-resolution powder bed fusion (PBF) additive manufacturing techniques offer designers the ability to develop geometrically complete components from engineering materials with minimal geometrical constraints. PBF processes can produce commercial products from materials such as polymers, ceramics, composites and metals [9].

Titanium alloys are most commonly used by metallic 3D printers due to their excellent mechanical and biocompatibility properties. These properties also render titanium alloys a strong candidate for 3D printed biomedical implants. At present, 3D printed Ti-6Al-4V ELI alloy implants have been surgically implanted into the human body with promising results [10, 11].

2.1.1 Powder Bed Fusion (PBF) Manufacturing Techniques

The additive manufacture of most commercial metal parts is conducted by a PBF process. These techniques typically use either a laser or electron beam to fuse the material together to create the final build part [12]. These techniques are often used exclusively by the various manufacturers of the systems, and a short description of each technique is presented in Table 1:

Table 1 Comparison of Powder Bed Fusion (PBF) Techniques [13-16]

POWDER BED FUSION (PBF) TECHNOLOGY	MANUFACTURER	DESCRIPTION OF PROCESS
Direct Metal Laser Sintering (DMLS)	EOS GmbH	The metal powder is fused by the local heat of a focused laser sintering process. The system can only be used with metal powder.
Selective Laser Sintering (SLS)	3D Systems Corp.	The material powder is fused by the local heat of a focused laser sintering process. The system can be used for metals, ceramics and polymers.
Selective Laser Melting (SLM)	Concept Laser GmbH	The metal powder is fully melted by a focused laser beam to fuse powder to form a homogeneous part. The system can only be used with metal powder.
Electron Beam Melting (EBM)	Arcam AB	The metal powder is fully melted by a focused electron beam to fuse powder to form a homogeneous part. The system can only be used with metal powder.

Titanium alloys are well suited to additive manufacturing techniques because of the difficulties in performing traditional machining operations. Titanium is a poor thermal conductor, causing the material to retain heat in the specific areas being machined which results in work hardening of the surface. As a result of the higher cutting forces and temperatures being required, damage and failure of the cutting tools are common during machining [17]. These issues make additive manufacturing a desirable alternative for components which contain complex geometries.

SLM and EBM are the most commonly used additive manufacturing technologies for the fabrication of titanium components. For comparison, the main differences between the Arcam A1 EBM and Concept Laser M2 SLM systems are outlined in Table 2:

Table 2 Differences Between EBM and SLM Manufacturing Techniques [18-22]

CHARACTERISTIC	ELECTRON BEAM MELTING (EBM)	SELECTIVE LASER MELTING (SLM)
Thermal Source	Electron Beam	Laser
Atmosphere	Vacuum	Inert Gas
Scanning Process	Deflection Coils	Galvanometers
Scanning Speed	8000 m/s	4 – 7 m/s
Energy Absorption	Conductivity-Limited	Absorptivity-Limited
Powder Pre-Heating	Electron Beam	Infrared Heaters
Power Requirements	7 kW	7.4 kW
Surface Finish	R_a 25 – 35 µm	R_a 9 – 12 µm
Feature Resolution	± 0.2 mm	± 0.1 mm
Build Times	55 – 80 cm^3/h	2 – 35 cm^3/h

SLM systems provide a better surface finish, feature size and resolution than EBM systems, however, the build times for SLM are significantly slower than EBM fabrication [18]. Additionally, parts manufactured using SLM contain high residual internal stresses which can only be removed by further heat treatment processes such as annealing [23]. Significant support structures are also required in the SLM process to allow for the transfer of heat away from the top surface. The density and compressive strength of EBM parts exceed those of SLM due to the formation of cracks and unmolten areas inside the SLM parts [24]. It is for these reasons that EBM fabricated components were selected for this investigation.

2.1.2 Electron Beam Melting (EBM)

Electron Beam Melting (EBM) is a powder bed fusion process which is used exclusively by Arcam AB in their 3D printing systems [16]. The process is similar to the more common Selective Laser Sintering (SLS) technology, however, the use of an electron beam results in faster build times and higher productivity [25]. The EBM technology builds fully dense objects to the specific geometry as defined by a CAD model. This process is predominantly used with Ti-6Al-4V powder which is supplied by the manufacturer Arcam AB.

During the building stage of the process, the chamber is evacuated and a partial pressure of helium is introduced. A vacuum environment is required to ensure the electrons are not deflected during the melting process, and also to ensure the final component is free from impurities and oxidation. The conductive metal powder is stored in two powder hoppers either side of the build platform. Prior to

melting, the powder is fed onto the build platform and is flattened by a rake to the desired layer thickness of the build (typically set to between 50 – 70 µm).

An electric current of 10 A (DC) drives a tungsten filament which operates at an anode potential of 60 kV [26]. This provides the electron gun with up to 4 kW of power to melt the metallic powder on the build platform. An initially unfocused scan of the electron beam across the powder preheats and sinters the powder. The high-powered electron beam is then focused onto the powder bed through a series of three magnetic lenses; the astigmatism lens, the focus lens and the deflection lens. The first lens is used to adjust for astigmatism and to generate a circular electron beam with a Gaussian energy distribution [27]. The focus lens is responsible for focusing the electron beam into a small localised circle which is then deflected by the deflection lens, allowing the electron beam to scan across the entire build surface. The electron beam can operate at a scanning speed of up to 8000 ms^{-1} [19]. Arcam *Multibeam™* technology allows this process to occur simultaneously across multiple melt pools to increase efficiency and reduce build times [16].

The outline contours of the cross-section are melted first to ensure a strong shell of the component, followed by the insides of the cross-section. The powder is melted by an automatically controlled electron beam current and scanning speed as defined by the build instructions [26]. After a layer has been fully melted, the build platform will drop down by the pre-defined layer height and the process will be repeated for the new cross-section. The scan path of the electron beam follows a raster pattern which defines the direction and spacing of the electron beam path. The direction of the scan path will shift 90° after each layer to ensure an even melt of the powder occurs.

The final stage is the post-processing phase of the EBM manufactured part. The excess powder is removed by blasting the part with compressed air inside a glove box chamber. This powder can be recycled and reused inside the system for another build. Other post-processing techniques are required to remove support material and increase the quality of the surface finish of the part. A schematic diagram of the Arcam EBM system is shown in Figure 1:

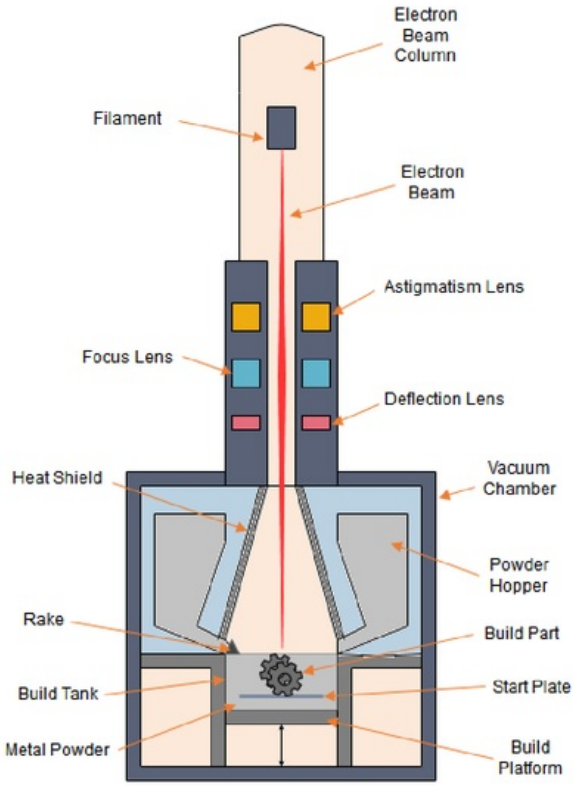

Figure 1 Schematic Diagram of Arcam A1 EBM System

2.2 Titanium 6-4 (Ti-6Al-4V) ELI Alloy

2.2.1 Material Properties

Titanium materials are well suited to a diverse range of applications due to their excellent material properties such as high strength, low density and high corrosion resistance. Titanium materials also exhibit good biocompatibility which makes this material an attractive choice for orthopaedic applications.

Pure titanium cannot be heat treated and has a lower mechanical strength than the various titanium alloys. Titanium 6-4 (Ti-6Al-4V) alloy is one of the most popularly used titanium alloys and is often referred to as the 'workhorse' of the titanium industry as it accounts for over 50 % of all titanium used worldwide [28]. Ti-6Al-4V alloy has many applications in the biomedical, aerospace and automotive industries. Titanium 6-4 ELI (Ti-6Al-4V ELI (Extra Low Interstitials)) [ASTM Grade 23] is an alloy of higher purity than standard Ti-6Al-4V [ASTM Grade 5], which contains reduced levels of oxygen, nitrogen, carbon and iron. Ti-6Al-4V ELI also offers greater ductility and improved fracture toughness than standard Ti-6Al-4V [29].

Titanium alloys are grouped into alpha (α), beta (β) or alpha-beta (α + β) microstructural categories and graded based on the chemical composition of the alloy. The room temperature α phase grains form a hexagonal close-packed (HCP) structure and the aluminium component of the alloy acts as an α stabiliser which increases the temperature at which the α phase is stable [30]. The β phase grains form a body-centred cubic (BCC) structure and the addition of vanadium acts as a β stabiliser which results in the increased stability of the β phase at lower temperatures [30]. Higher yield strengths are attributed to α phase grains which contain a more refined lamellar structure [31, 32].

Ti-6Al-4V ELI is an α + β phase alloy which contains both α and β grains in a dual-phase lamellar grain microstructure. Due to the high cooling rate of the EBM process, the resulting microstructure of the Ti-6Al-4V ELI material is mainly composed of α phase grains in a β phase grain matrix [32]. During cooling, the β phase grains transform into α phase grains at the beta transus temperature which occurs at approximately 883 °C. The typical chemical composition of Arcam Ti-6Al-4V ELI powder in comparison with cast Ti-6Al-4V materials (in wt. %) is shown in Table 3:

Table 3 Typical Chemical Composition of Arcam Ti-6Al-4V ELI Powder and Cast Ti-6Al-4V Materials

ELEMENT	ARCAM Ti-6Al-4V ELI POWDER (GRADE 23) [max. wt. %] [29]	CAST Ti-6Al-4V ELI (GRADE 23) [max. wt. %] [33]	CAST Ti-6Al-4V (GRADE 5) [max. wt. %] [34]
Aluminium	6	5.5 – 6.75	5.5 – 6.75
Vanadium	4	3.5 – 4.5	3.5 – 4.5
Oxygen	0.15	0.13	0.2
Iron	0.1	0.25	0.3
Carbon	0.03	0.08	0.1
Nitrogen	0.01	0.05	0.05
Hydrogen	0.003	0.0125	0.0125
Titanium	Balance	Balance	Balance

EBM manufactured components built from Arcam Ti-6Al-4V ELI alloy powder have superior mechanical properties to cast and wrought materials. The typical Ultimate Tensile Strength (UTS or σ_{UTS}) and Yield Strength (YS or σ_{YS}) of EBM Ti-6Al-4V are significantly higher than cast materials and comparable with wrought materials. The Young's modulus of elasticity is also higher for the EBM manufactured components. The mechanical properties of EBM manufactured, cast and wrought Ti-6Al-4V ELI are compared in Table 4:

Table 4 Mechanical Properties of Typical Ti-6Al-4V ELI Materials

MECHANICAL PROPERTIES	ARCAM EBM Ti-6Al-4V ELI [29]	CAST Ti-6Al-4V ELI [35]	WROUGHT Ti-6Al-4V ELI [36]
Yield Strength (YS or σ_{YS})	930 MPa	758 MPa	860 MPa
Ultimate Tensile Strength (UTS or σ_{UTS})	970 MPa	860 MPa	930 MPa
Elongation	16 %	> 8 %	> 10 %
Rockwell Hardness	32 HRC	30-34 HRC	30- 35 HRC
Young's Modulus of Elasticity	120 GPa	105-120 GPa	114 GPa

2.2.2 Biocompatibility of Titanium 6-4 ELI Alloy

Extensive studies by Geetha *et al.* [37] and Shah *et al.* [38] have verified the biocompatibility of commercially pure Ti-6Al-4V ELI for both *in vitro* and *in vivo* tests. At present, Ti-6Al-4V ELI is the most common titanium material for biomedical applications [37]. In recent times, the rapid proliferation of the additive manufacturing sector has allowed for the development of 3D printed biomedical

implants. However, there has been a lack of studies conducted on the biocompatibility of 3D printed materials, as their biocompatibility has often been assumed to be the same as traditional wrought or cast materials.

A recent study by Shah *et al.* [39] has indicated that although EBM manufactured Ti-6Al-4V promoted cellular attachment and proliferation, the interfacial tissue between implant and bone was found to be less mature than the native bone after a period of prolonged healing. This is of significant concern for biomedical applications and suggests that further work in this area is necessary to confirm the biocompatibility of 3D printed implants.

2.3 Thin Film Material Deposition

2.3.1 Diamond-Like Carbon (DLC) Coatings

Diamond-like carbon (DLC) is an amorphous form of carbon, which contains a high proportion of carbon atoms in hybridised sp^3 bonds [40]. The sp^3 bonding is the type of bonding which is found in the diamond form of carbon. This bonding structure allows the DLC material to exhibit a high mechanical hardness, high modulus of elasticity and high wear resistance [40, 41]. DLC is an FDA approved biocompatible material that is chemically inert and offers mechanical flexibility with tunable compositions which allows for its use in many applications.

Carbon exists in three distinct hybridised structures; sp, sp^2 and sp^3. In the sp^3 configuration, the four valence electrons of carbon are arranged in a tetrahedral fashion. This type of configuration forms a strong bond with adjacent atoms, which gives the diamond material its characteristic mechanical properties [40].

DLC is a thin film material that is often deposited as a protective coating on a material substrate for tribological applications such as automotive parts, biomedical implants and cutting tools. The addition of dopants to the DLC coating allows for greater functionality and properties for specific applications. The typical mechanical properties and functionality of DLC coatings are shown in Table 5:

Table 5 Typical Mechanical Properties and Functionality of DLC Coatings

COATING	DOPANT (AT. %)	MECHANICAL HARDNESS	ELASTIC MODULUS	FUNCTIONALITY
DLC	0	17 GPa	155 GPa	Hard, Wear-Resistant, Lubricious
F-DLC	3-24	15-19 GPa	85-150 GPa	Anti-Fouling, Anti-Bacterial, and Hydrophobic
Si-DLC	4-24	12-13.5 GPa	105-115 GPa	Enhanced Mechanical Stability and Lower Coefficient of Friction

The favourable mechanical properties of DLC such as a low coefficient of friction and high wear resistance make the material a good candidate for biomedical applications such as joint replacement arthroplasty. Extensive studies have also confirmed the biocompatibility of DLC coatings *in vitro*, for cell interactions such as fibroblasts and osteoblasts.

In a study by Kim *et al*. [42], DLC coatings have been successfully deposited onto Ti-6Al-4V materials with promising results. The study also indicated that DLC coatings significantly enhanced the wear

properties of commercially pure Ti-6Al-4V [42], however, there is limited evidence in the literature on the effects of DLC coatings deposited onto 3D printed material substrates.

2.3.2 Plasma Activated Chemical Vapour Deposition (PACVD)

DLC coatings are most commonly deposited on metal substrates using plasma activated chemical vapour deposition (PACVD). This process uses a controlled chemical reaction to deposit a conformal thin film coating onto a material substrate.

In PACVD, an uncoated material is placed onto an electrode (substrate holder) inside an evacuated chamber. A radio frequency (RF) power supply is used to apply an RF oscillating voltage to the electrode which generates a plasma inside the vacuum chamber. Precursor and reaction gases are then pumped into the chamber at a controlled flow rate. During this time, the plasma transfers energy to the gas mixture by electron impact, which initiates ionisation and dissociation of the gas particles. The gas reactants are then transported to the substrate of the material by diffusion. The gas reactants form the reaction products and are adsorbed onto the surface into a conformal thin film coating [43].

Plasma etching of the material substrate is performed using argon gas to remove oxide, hydrocarbons and other contaminants from the substrate prior to coating. In order to improve the adhesion of the DLC coating, a thin layer of hydrogenated amorphous silicon carbide (a:SiCH) is first deposited onto the substrate using tetramethylsilane gas ($Si(CH_3)_4$). The a:SiCH layer allows for strong adhesion between the substrate and the DLC film. The DLC coating is deposited using acetylene gas (C_2H_2). A schematic diagram of the PACVD system is shown in Figure 2, and an image of the glowing plasma discharge is shown in Figure 3:

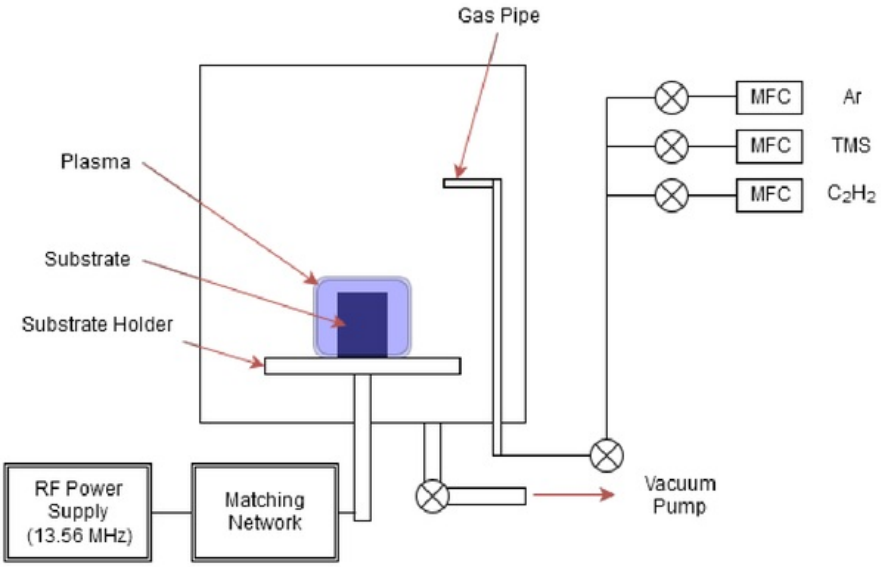

Figure 2 Schematic Diagram of RF PACVD System

Figure 3 Example of Plasma Discharge Glow inside the PACVD Vacuum Chamber

2.4 Characterisation of Materials

Material characterisation is important for understanding the chemical composition, bonding and structure of a material. A range of characterisation techniques is required to gain an in-depth insight into how the bulk of the material behaves in comparison to the surface of the material.

2.4.1 White Light Interferometry (WLI) Measurement

White light interferometry (WLI) is a non-contact optical method for measuring 3D surface topography to obtain surface roughness measurements. Interferometry techniques are based on the principle of wave superposition in which separate light waves are combined to measure changes occurring to either wave [44]. In WLI measurement, a light ray is split by a partial mirror which separates the light ray into two identical light beams which travel in different directions. These light beams are then recombined at a detector, and the difference in path lengths results is a phase change between the beams. In Vertical Scanning Interferometry (VSI), the light reflected from a sample is combined with light from a reference mirror to produce interference fringes which can be reconstructed to produce information about the sample material [44, 45].

2.4.2 Scanning Electron Microscopy (SEM) Imaging

Scanning electron microscopy (SEM) is a performed using an electron microscope which uses a focused electron beam to produce images of high resolution and magnification. During SEM imaging, an electron beam is generated inside a vacuum chamber and is deflected by a series of coils to rapidly scan the surface of a material. The interaction between the high-energy electrons and sample results in the excitation of atoms which produces a variety of signals. For imaging, secondary electron signals are collected by a detector which is used to produce an image of the surface topography.

2.4.3 Energy Dispersive X-Ray (EDX) Spectroscopy

Energy Dispersive X-Ray (EDX) spectroscopy is a material characterisation technique which is often used in conjunction with SEM to perform elemental composition analysis. In EDX spectroscopy, an electron beam is used to penetrate the surface atoms of materials causing the ejection of an electron

from a lower energy state. The ejected electron is then replaced by an electron from a higher energy state which releases its excess energy in the form of characteristic X-Rays [46]. These X-Rays are then detected by a solid state detector (SSD) which generates a spectrum that can be analysed to characterise the material at a detection depth of 1 µm.

Quantitative elemental composition analysis of materials is calculated using the Castaing's approximation formula, which assumes that the relative intensity of an X-Ray line is approximately proportional to the mass concentration of the target element [47]. This relationship can be used to derive an 'approximate concentration' of each element using the following equation:

$$C' = \left(\frac{I_{sp}}{I_{st}}\right) C_{st}$$

Where C' is the 'approximate concentration', I_{sp} is the intensity of the element peak, I_{st} is the intensity of the peak of the carbon element (which is the reference standard) and C_{st} is the concentration of the carbon reference standard. Further corrections such as a background correction are also required to increase the accuracy of the results, which has a statistical precision of ± 1%.

2.4.4 X-Ray Photoelectron Spectroscopy (XPS)

X-Ray Photoelectron Spectroscopy (XPS) is a surface characterisation technique in which a material surface is irradiated by monoenergetic X-rays of the MgKα (1253.6 eV) line to excite electrons in the surface region. This causes photoelectrons to be emitted due to the photoelectric effect. A photoelectric spectrum is produced by counting the number of emitted photoelectrons over a range of electron kinetic energies [48]. The resulting photoelectric spectrum can then be used to characterise the surface composition and chemical state of the materials at a detection depth of 3-5 nm. Quantitative elemental composition can be determined using the intensity of the peaks I, of any element x, using the following relationship:

$$C_x = \frac{\frac{I_x}{S_x}}{\sum_i \left(\frac{I_i}{S_i}\right)}$$

Where S is the sensitivity factor which compensates for the fact that the detector does not have the same ability to detect electrons from different energy levels and elements [49].

2.4.5 Low Energy Ion Scattering (LEIS) Spectroscopy

Low Energy Ion Scattering (LEIS) is a surface characterisation technique in which a beam of low-energy helium ions (He^+) is used to bombard the surface of a material. The helium ions collide with the surface atoms in the substrate and are reflected back at different kinetic energies due to the momentum transfer between the incident ion and the surface atoms. The change to the kinetic energy corresponds to the specific atomic mass of the elements which are present [50]. This allows us to determine which elements are present and their corresponding atomic fractions. The LEIS technique is an extremely sensitive surface characterisation technique and can be used to characterise the sample materials at a detection depth of one atomic layer.

The energy spectrum of the scattered ions from the surface reveals peaks which correspond to the specific target atoms in the material surface. The relationship between the energy of the ion before and after collision is defined by the following equation [51]:

$$E_F \equiv kE_0$$

$$E_F = \left(\frac{\cos\theta + \sqrt{r^2 - \sin^2\theta}}{1 + r}\right)^2 E_0$$

Where k is the kinematic factor, E_0 is the primary ion energy, r is the ratio between the target atom mass and the He^+ ion mass, and ϑ is the scattering angle of the incident He^+ ions.

A calibration curve is used to quantify the elemental composition based on known relationships of pure elements. Using the calibration data, we are able to calculate the approximate composition of the surface by correcting the intensity of the final energy of the ion for the differences in atomic radii of the surface elements [51]. The calibration curve we used is shown in Figure 4, the solid red line is the calculation according to the scattering equation and the solid points are measurements taken from standard materials of known mass.

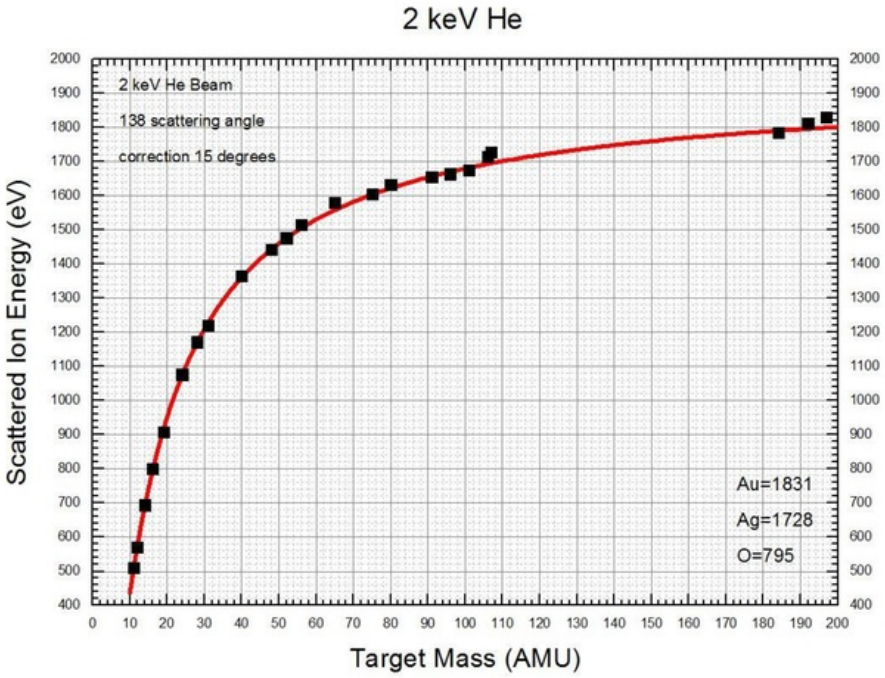

Figure 4 Calibration Curve Used For LEIS Analysis

2.4.6 Surface Wettability

Wettability is the preference of liquid to favour one fluid over another and is a study of how a liquid spreads out when in contact with a solid substrate [52]. The contact angle is the angle that is formed by the intersection of the liquid-solid interface and the liquid-vapour interface (geometrically acquired by applying a tangent line from the contact point along the liquid-vapour interface in the droplet profile) [53]. An illustration of the principle is shown in Figure 5:

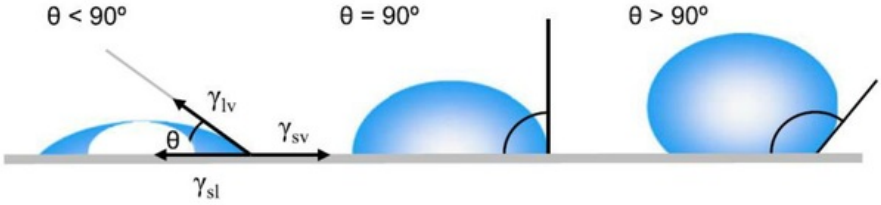

Figure 5 Example of Contact Angle Measurements [53]

When conducting contact angle measurements with distilled water, a measurement of less than 90° indicates that wetting of the surface is favourable and considered hydrophilic. In contrast, a contact angle measurement of greater than 90° indicates that wetting is unfavourable and the surface is considered hydrophobic [53]. Contact angle measurements can also be performed other fluids in conjunction with water to develop a more comprehensive understanding of the surface hydrophobicity.

2.5 Tissue Engineering and Additive Manufacturing

Tissue engineering is concerned with the study and development of scaffolds, cells and biologically active molecules into functional tissue [54]. A key challenge in this field is to generate biomaterials which can successfully provide physical and local environments that facilitate tissue development [55]. The specific design of these scaffolds is critical in tissue engineering to ensure that an implant can successfully promote cell adhesion, proliferation and differentiation [56].

Additive manufacturing is well suited to biomedical applications because of the large degree of customisation that can be incorporated into component designs. Modern additive manufacturing techniques allow biomaterials to be specifically engineered to contain macro and micro-architecture which promotes cellular interaction with existing body tissue. Precise control of these structures is vital to ensure that the implant is successful, especially for more complex biomedical applications such as craniomaxillofacial or spinal implants. The complex geometry of these structures cannot be easily controlled with traditional manufacturing techniques.

2.5.1 Biomaterials for Orthopaedic Applications

A biocompatible material is defined by the U.S National Institutes of Health (NIH) as "*any substance (other than a drug) or combination of substances synthetic or natural in origin, which can be used for any period of time, as a whole or part of a system which treats, augments, or replaces tissue, organ, or function of the body*" [57].

A review by Navarro *et al.* [58] has suggested that there exist three generations of biomaterials which can describe the present research and development in this field. These generations are defined as:

- ***First Generation:*** Materials which are biologically inert and non-toxic to the human body.
- ***Second Generation:*** Materials which are biologically active and biodegradable.
- ***Third Generation:*** Materials which have been engineered to promote and stimulate cellular responses at the molecular level.

Ti-6Al-4V ELI alloy can be considered a first generation biomaterial due to the material's well-documented biocompatibility, and bio-inertness. However, additive manufacturing has evolved this material into a third generation biomaterial because of the ability to design and engineer macro structures. These structures are often used to stimulate a specific cellular response to assist in the healing and regeneration of the surrounding body tissue.

Surface coatings can also be considered a form of a third generation biomaterial as they can be engineered to promote cellular responses and inhibit the growth of harmful bacteria. These coatings have significant potential for 3D printed Ti-6Al-4V ELI as there are concerns that wear debris from implants can cause leaching of aluminium and vanadium, which is potentially cytotoxicity to the body [4].

2.6 Biological Analysis of Materials

2.6.1 Saos-2 Human Osteosarcoma Cell Line

Saos-2 is a cell line which has been derived from human bone osteosarcoma (malignant bone tumour) cells, and are commonly used for osteoblastic models *in vitro* [59]. Bone cell osteoblasts are responsible for the formation of new bone tissue and are a result of osteogenic cell differentiation. Saos-2 cells exhibit osteoblastic behaviour *in vitro*, and also possess the ability to mineralise in osteogenic media [60].

Saos-2 cells were used in all biological assays as they are recognised to be a robust *in vitro* model for bone cell behaviour that occurs *in vivo* [55, 59]. We studied the following three aspects of the cell response for comparing our materials and in order to validate our hypothesis:

- Cell adhesion and growth/proliferation on samples over 7 days.
- Cell differentiation and mineralisation on samples over 28 days.

2.6.2 Cytotoxicity of Materials

Cytotoxicity is a measure of the toxicity of a material to healthy cells, a major concern for the biocompatibility of a material. Indirect cytotoxicity testing is conducted to screen for the presence of any toxic compounds in the media.

2.6.3 Cell Adhesion and Proliferation

Cell adhesion allows cells to attach to a material surface and can lead to further cellular activities. Successful cell adhesion allows for the cell to spread out resulting in a change in cell morphology, as shown in Figure 6. The adherence of cells to a surface *in vitro* is controlled by exposing surfaces to culture media containing serum which results in the formation of a thin monolayer comprised mainly of proteins that adsorb to the material surface [61]. Cells must be maintained at the appropriate temperature (37 °C), humidity (100 %) and pH (7.2) in order for healthy cell development to occur [62].

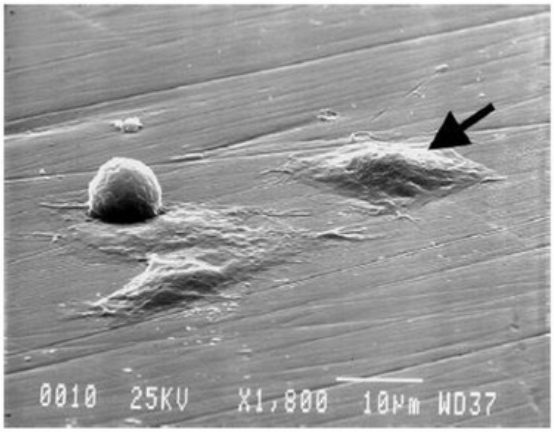

Figure 6 Example of Cells at Various Stages of Adherence Demonstrating Changes in Cell Morphology [61]

Mitosis is a distinctive cell cycle phase in which a parent cell is divided into two daughter cells, and the replicated chromosomes are separated into two new cell nuclei [63]. This process is concurrently accompanied by cytokinesis which is the physical process of dividing the cytoplasm, organelles and cell membrane into the two new daughter cells.

In Saos-2 cells, these processes occur at approximately a 2 to 3-fold greater mean doubling-time at a 15 to 20-fold higher saturation density than that of human osteoblasts [59]. Cell proliferation is the rate at which the number of cells is increasing over a period of time.

2.6.4 Cell Mineralisation

Mineralisation is the biological process in which osteoblasts (bone-forming cells) mature/differentiate and produce calcium phosphate crystals [64]. Active osteoblasts secrete extracellular bone matrix molecules which form the connective scaffolding that holds tissue together. When osteoblasts become trapped in the extracellular matrix that they secrete, they become osteocytes. Osteocytes are considered to represent the terminal differentiation phase of osteoblasts [60].

Mineralisation testing involved the use of an *in vitro* mineralisation assay with cells to monitor and assess the differentiation and maturation of cells adherent to a substrate over a period of 28 days. Differentiation products are quantitatively measured, with alkaline phosphatase (ALP) used as an initial indicator of differentiation, and calcium as an indicator of the later stage of differentiation.

3. Methodology

3.1 Test Materials

Our EBM parts were manufactured from a CAD model which was produced using the PTC *Creo Parametric 2.0* Computer Aided Design (CAD) software package. The *Creo Parametric 2.0* software was also used to convert the original PRT file into an STL file which was used for EBM manufacturing. The dimensions of the EBM manufactured test samples is shown in Figure 7:

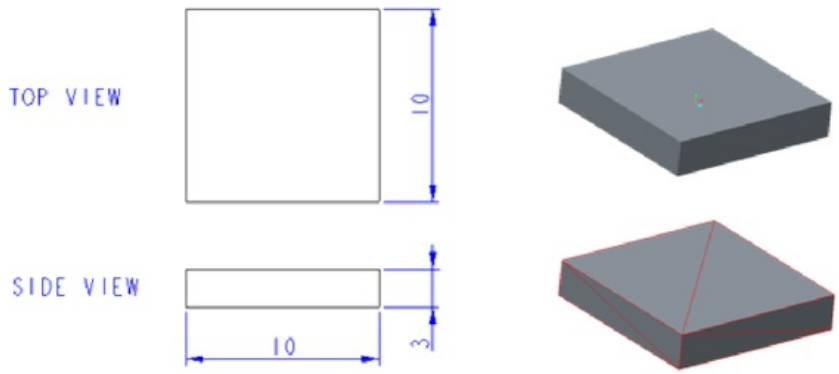

Figure 7 Left: Dimensions of 3D Printed Test Samples (In Millimetres). Right: CAD and STL Models of Test Samples

In order to test our hypothesis that we can enhance the biocompatibility of 3D printed Ti-6Al-4V ELI alloy, we compared the following materials in our experiments as presented in Figure 8:

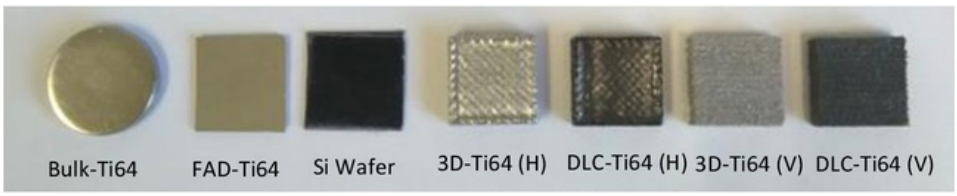

Figure 8 Test Material Samples

Table 6 Test Materials and Codes Used For Experiments

TEST MATERIAL	CODE USED
EBM Manufactured Ti-6Al-4V ELI (Horizontally Built)	3D-Ti64 (H)
EBM Manufactured Ti-6Al-4V ELI (Vertically Built)	3D-Ti64 (V)
DLC on Ti-6Al-4V ELI (Horizontally Built)	DLC-Ti64 (H)
DLC on Ti-6Al-4V ELI (Vertically Built)	DLC-Ti64 (V)
Bulk Ti-6Al-4V (Commercially Produced)	Bulk-Ti64
Ti-6Al-4V (Filtered Arc Deposited [FAD] on Si Wafer)	FAD-Ti64
Silicon Wafer (Commercially Produced)	Si Wafer
Tissue Culture Polystyrene (TCPS Control for Biological Testing)	TCPS

For material characterisation of our EBM manufactured samples, we included a bulk and Filtered Arc Deposited (FAD) Ti-6Al-4V on silicon wafer sample as control materials for our experiments. Our biological experiments were conducted on both DLC coated and as-built EBM manufactured Ti-6Al-4V ELI samples to compare the biocompatibility of each material. We also included FAD Ti-6Al-4V, silicon wafer and Tissue Culture Polystyrene (TCPS) samples as control materials for our biological experiments. TCPS is a standard control material for all biological experiments. We also included the FAD Ti-6Al-4V and silicon wafer samples in our in our biological experiments as a comparison material for our EBM manufactured samples which contains a surface roughness in the nanoscale.

3.2 Electron Beam Melting (EBM)

An Arcam A1 EBM system was used to manufacture our samples for this project. The samples were manufactured in both a horizontal and vertical direction (as shown in Figure 9) for comparison, using Ti-6Al-4V ELI power with a particle size of 50 – 70 µm supplied by Arcam AB (Mölndal, Sweden) as the feedstock material. The process was performed in an inert helium environment at a vacuum pressure of 2 x 10^{-3} mbar. The build temperature was maintained at 700 °C, with a starting plate temperature of 730 °C, and an electron beam diameter of 0.2 mm.

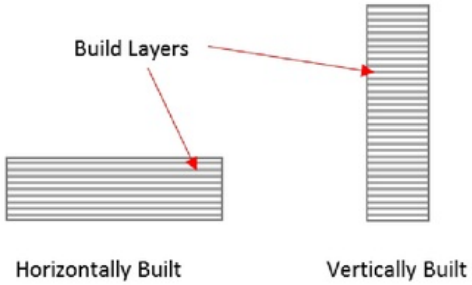

Figure 9 Description of Build Orientation of EBM Manufactured Parts

Figure 10 CSIRO's Arcam A1 EBM Machine

3.3 Thin Film Material Deposition

3.3.1 Cleaning and Preparation of Material Samples

All samples were cleaned prior to thin film coating using ultrasonic cleaning and a three-stage solvent process. The samples were first washed in an X55 solvent solution for 15 minutes, then washed in an acetone solution for 15 minutes, and finally washed in an ethanol solution for a further 30 minutes. The samples were then dried with nitrogen gas and placed in a sealed petri dish.

3.3.2 Plasma Activated Chemical Vapour Deposition (PACVD)

All samples were placed into the vacuum chamber of the PACVD system, which was pumped down using a turbomolecular pump to a base pressure of approximately 6-9 x 10^{-6} mbar. Argon gas was initially fed into the chamber at a flow rate of 10 cm^3/min to reach a gas pressure of 3 x 10^{-2} mbar in order to perform plasma etching. The plasma etching process was initiated by switching the RF power to 200 W for 10 minutes. Directly following the etching process, an interlayer of amorphous silicon carbide (a:SiCH) was deposited by introducing tetramethylsilane (TMS) into the chamber at the flow rate of 40 cm^3/min to reach a working gas pressure of 3 x 10^{-2} mbar and then the RF power supply was set at 200 W for 5 minutes, resulting in a layer thickness of approximately 100 nm. The silicon carbide layer was deposited in order to improve the adhesion of the DLC film. Finally, the DLC layer was deposited using acetylene (C_2H_2) gas which was fed into the chamber at a flow rate of 100 cm^3/min to reach a working pressure of 6 x 10^{-2} mbar. The deposition time of the DLC layer was set at 15 minutes at 200 W RF power. The DLC coating thickness was measured to be approximately 1 µm.

Figure 11 CSIRO's RF Plasma Activated Chemical Vapour Deposition (PACVD) System

3.3.3 Filtered Arc Deposition

Silicon wafer substrates were placed into a custom-built filtered arc deposition system which was pumped overnight to a base pressure of 2 x 10^6 mbar. To initiate the process, a plasma was ignited on the Ti-6Al-4V cathode target with an arc current of 110 A. The ionised metal beam was directed to the sample stage which was biased at 100 V and was deposited for 5 minutes to form a 1.2 µm Ti-6Al-4V film on the silicon substrates. The FAD system used for this project is shown in Figure 12:

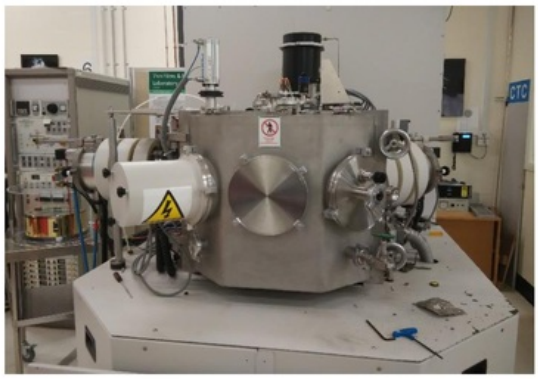

Figure 12 CSIRO's Custom-Built Filtered Arc Deposition (FAD) System

3.4 Characterisation of Materials

3.4.1 X-Ray Diffraction (XRD) Analysis

The XRD analysis was conducted with a Cu K_α source using a PANanalytical X'Pert Pro Materials Research Diffractometer (MRD) system.

3.4.2 White Light Interferometry (WLI) Measurement

WLI measurements were conducted by using the Bruker-AXS NT-9800 optical surface profiler instrument with a 0.80 numerical aperture and 5x Michelson objective. The measurement was performed at Macquarie University.

3.4.3 Scanning Electron Microscopy (SEM) Imaging

SEM was conducted using a Zeiss Auriga SEM instrument at CSIRO Lindfield. Images were captured from a 15 keV electron beam energy with an InLens secondary electron detector.

3.4.4 Energy Dispersive X-Ray (EDX) Spectroscopy

EDX spectroscopy was measured using an Oxford Instruments X-Max solid-state SSD attachment for the Zeiss Auriga SEM instrument with a 15 keV electron beam. The EDX analysis was performed using the Oxford Instruments *AZtecEnergy* software package.

3.4.5 X-Ray Photoelectron Spectroscopy (XPS)

Surface characterisation analysis using XPS were recorded using a SPECS Sage 150 system, with the MgKα line at 1253.6 eV used as the excitation source. Both survey (step size of 0.5 eV) and high-resolution binding energy scans (step size of 0.1 eV) were conducted.

3.4.6 Low Energy Ion Scattering (LEIS) Spectroscopy

The LEIS measurements were recorded with a SPECS PHOIBOS 100 hemispherical analyser (HSA) using a 2 keV helium ion source with a 138° scattering angle and a 15° out-of-plane angle of the HSA.

3.4.7 Surface Wettability

The surface wettability of each sample was determined by contact angle measurements. Contact angle measurements were obtained by analysing photographic images of a 5 µL sessile water droplet placed on each sample using a pipette. A digital camera with a macro lens was used to take images of the drop profile which were later analysed in the open-source program *ImageJ*. An example image of the contact angle measurement is shown in Figure 13.

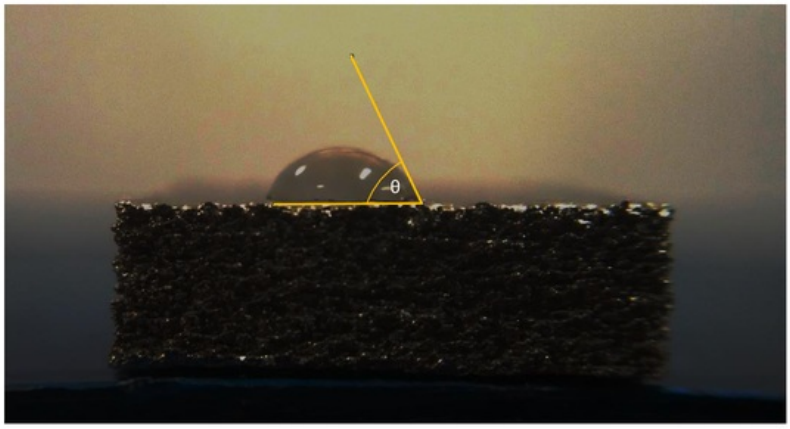

Figure 13 Example of Contact Angle Measurement of 3D-Ti64 (V) Sample using ImageJ

3.5 Biological Testing of Materials

3.5.1 Sterilisation of Sample Surfaces

Prior to conducting the biological assays, all samples were sterilised to remove any biological agents from the surface of our test materials. For sterilisation, both sides of each sample were exposed to ultraviolet (UV) radiation for 30 minutes. After this point, all procedures were conducted in a Class II biohazard cabinet under aseptic conditions.

3.5.2 Cell Adhesion and Proliferation Assay

Cell adhesion and proliferation assays were used to determine the initial rate of cell adhesion to the test substrates and the rate of growth of those cells over a 7-Day time period. At time-points at Day 1, 4 and 7 cell numbers were measured by microculture tetrazolium (MTT) cell viability assay. A total of 16 samples of each test surface were used for this assay. For the cell adhesion study, two samples were used at each of the two time-points of 24 and 48 hours. For the cell proliferation assay, three samples were used for MTT assay and one sample was used to check cell morphology at each of the three time-points of days 1, 4 and 7.

3.5.2.1 Set-Up of Proliferation Assay

Prior to Day 1 of the assay, test samples were placed into individual wells of 24-well TCPS plates. For each sample type, a total of 16 samples [(2 x 2) + (3 x 4)] was set-up for the various assays. Saos-2 cells were seeded at a concentration of 5×10^4 cells/mL in a volume of 1 mL directly onto each sample in standard cell culture medium SM-DMEM/Hams F12 supplemented with 10 % (v/v) foetal bovine serum, penicillin (100 U/mL), streptomycin (100 µg/mL) and L-glutamine (200 mM). Plates were incubated at 37 °C in humidified air containing 5 % carbon dioxide (CO_2) to allow cells to attach and spread on the substrates.

3.5.2.2 Cell Adhesion

Cell adhesion was measured after both 24 and 48 hours, by removing two samples from each sample set which were then fixed in 4 % formal saline in phosphate-buffered solution (PBS) for 30 minutes at room temperature. The samples were then examined for cell attachment and spread using fluorescent microscopy.

3.5.2.3 Imaging of Cells Surrounding Samples

During seeding, some of the cells settled on test samples and also on the surface of the TCPS well around each test sample. Images were taken of cells that settled around each set of samples of cells to check cell morphology as an additional check for cytotoxicity.

3.5.2.4 Cell Proliferation

After 24 h of the proliferation assay, three samples from each sample set were removed from the incubator to measure the number of adherent cells for the cell proliferation assay. Each sample was transferred to the well of a fresh plate and an MTT assay was conducted to gather Day 1 data. This was conducted by adding 1.5 mL of MTT solution at a concentration of 500 µg/mL in SFM with Internal Transcribed Spacer (ITS) to each well. The plates were incubated for 4 h at 37 °C in humidified air containing 5 % CO_2.

The culture medium was then removed from the wells of the plate and 1 mL of dimethyl sulfoxide (DMSO) was added to each well. The plates were then shaken gently for 10 minutes at room temperature to dissolve the blue formazan product. A 100 µL representative sample was then transferred to a 96-well plate for measuring optical density using a Plate Reader which was set at a wavelength of 595 nm. The entire process was repeated again on Day 4 and Day 7 of the assay. The culture medium was replenished on Day 4 for wells remaining to Day 7.

The mean values were calculated from triplicate wells of each sample at each time-point and data adjusted to take into account the difference in area between test samples (1 cm^2) and TCPS wells (2 cm^2) so they could be compared.

3.5.2.5 Fluorescent Staining of Cells

On Day 7, one sample from each of the sample sets and a TCPS control was stained with Cell Tracker Green (CTG) which was diluted at 1/1000 in SFM for 30 minutes to check cell morphology. CTG is a fluorescent tag that stains only living cells. After staining, the samples were fixed in 10 % formal saline in PBS for 30 minutes then stored until viewed. The samples were viewed using a microscope with a fluorescent light source and representative digital images collected for us to check the cell cover on each sample.

3.5.2.6 SEM Imaging of Cells

Samples were retained and stored in 100 % ethanol at 4 °C for later analysis by SEM to enable examination of the cell-material interactions. In order to preserve cell morphology for SEM imaging, critical point drying (CPD) of our samples was performed at Macquarie University. Samples were dried using an Emitech K850 CPD system using CO_2 for 2 hours at critical point (31.1°C and 739 bar).

3.5.3 Cell Differentiation and Mineralisation Assay

Alkaline Phosphatase (ALP) and calcium production of cells on each surface were measured as a quantitative measure of cell differentiation. ALP is used as an early indicator of differentiation where cells are still proliferative and calcium as an indicator of the later stage of differentiation in which mineralisation occurs. An MTT-based cell proliferation assay was also run concurrently to allow data outputs to be corrected for the number of cells adherent to each substrate.

3.5.3.1 Set-Up of Differentiation and Mineralisation Assays

Prior to Day 1 the assay, ten samples of each surface were placed into individual wells of 24-well plates and seeded with Saos-2 cells at a concentration of 3×10^4 cells/cm^2 in standard culture medium and incubated undisturbed for 4 days. Three replicate series of plates were established; two for the differentiation/mineralisation assay and one for the cell proliferation assay that was run in parallel. There were triplicate samples of each surface included in each plate with one extra included for imaging using CTG staining.

3.5.3.2 Cell Proliferation Assay

Cell proliferation was also measured in differentiated and undifferentiated culture regimes at Day 23 using a routine MTT assay (as previously described), which was conducted in parallel with the differentiation assay. All MTT results were adjusted for differences in areas of wafers/wells and normalised to values for cells grown in TCPS control wells under undifferentiated and differentiated culture regimes. This enabled the differentiation/mineralisation data (ALP and calcium) to be adjusted according to the number of cells attached to each substrate and TCPS controls at Day 23.

3.5.3.3 Fluorescent Staining of Cells

Cell coverage was examined on one representative wafer per set at Day 23 using the same process as outlined in the proliferation assay method.

3.5.3.4 Differentiation/Mineralisation Assay

Prior to the start of the differentiation/mineralisation assay, culture medium in one series of plates was replaced with the standard culture medium (undifferentiated control set samples) and in the other set of culture plates with osteogenic differentiation medium comprised by standard culture medium DMEM/Hams F12 in addition to the osteogenic supplements of β-glycerophosphate (1.5 mg/mL (7 mM)), dexamethasone (40 ng/mL (100 mM)) and ascorbic acid (20 µg/mL (70 µM)). The culture medium in both culture regimes was replenished every 3-4 days until assay stopped when mineral deposits were visible in the regime maintained on the osteogenic-specific differentiation culture regime which occurred at Day 23 in this assay. Differentiation was determined by measuring the production of both ALP and calcium in the adherent cells under both of the undifferentiated and osteogenic-specific culture regimes after 23 days.

3.5.3.5 Alkaline Phosphatase (ALP) Measurement

ALP was measured in cells adherent to the samples after 23 days using a quantitative assay based on p-Nitrophenyl Phosphate (p-NPP). We added 500 µL of p-NPP at a concentration of 2.0 mg/mL (0.1 M) in glycine buffer solution to each well containing a sample which was shaken for 60 minutes at 37 °C.

The reaction was neutralised by the addition of 500 µL (1 M) of sodium hydroxide (NaOH) per well. The optical density of wells containing test samples, controls and standards was read spectrophotometrically using a plate reader set at a wavelength of 405 nm. Sample sets were compared to a standard curve prepared from 10 µM/mL stock solution of p-NPP diluted in glycine buffer (0.1 M) solution and neutralised to create 8 standards ranging from p-NPP dilutions of 1/5 to 1/640.

3.5.3.6 Calcium Measurement

Calcium was evaluated using Arsenazo III which is a calcium sensitive dye, in a quantitative assay to determine the amount of calcium produced by cells adherent to each substrate after 23 days in culture.

Each sample was transferred to a fresh well and then we added 500 µL (0.6 M) of hydrochloric acid (HCl). The plates were then shaken at room temperature overnight to permeabilise cells and release the calcium. The reaction was neutralised the next day by the addition of 100 µL (3 M) NaOH per well. A 20 µL aliquot was taken from each well and mixed with 200 µL of Arsenazo III reagent at a concentration of 0.15 mg/mL to form a complex with the calcium which resulted in a colour change.

The optical density of the test samples, controls and standard wells was read spectrophotometrically using a plate reader set to a wavelength of 595 nm. Sample sets were compared to a standard curve prepared from 1 mg/mL calcium chloride ($CaCl_2$) stock solution diluted in water to create 8 standards ranging from $CaCl_2$ dilutions of 0 to 100 µg/mL.

3.5.3.7 Data Collection of Results

For both the ALP and calcium assays, the resulting values were adjusted to take in account the differences in sample areas and the control TCPS wells with final values expressed as either p-NPP mM/cm^2 or calcium mg/cm^2. Data was then normalised to the differentiated TCPS control value to give a percentage value and then corrected to take into account the number of cells present on surfaces as determined by the MTT assay run in parallel over the 23 day period.

4. Results

4.1 Characterisation of Materials

4.1.1 X-Ray Diffraction (XRD) Analysis

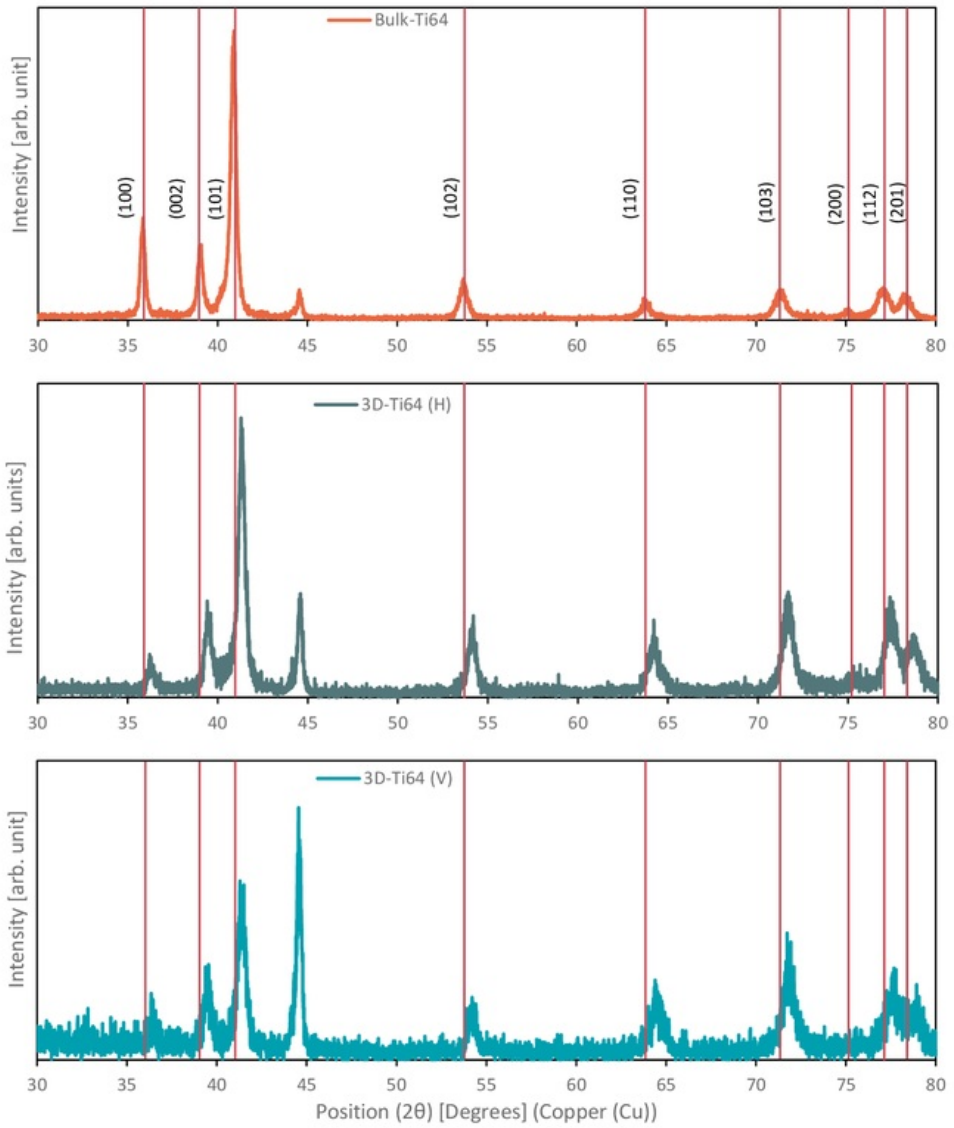

Figure 14 Top: XRD Pattern of Bulk-Ti64 Sample (with Labelled Miller Indices of Alpha Phase). Middle: XRD Pattern of 3D-Ti64 (H) Sample. Bottom: XRD Pattern of 3D-Ti64 (V) Sample.

The XRD patterns of the bulk Ti-6Al-4V shown on the top in Figure 14 indicate peak positions consistent with the expected result as presented in the literature [65, 66]. The EBM manufactured Ti-6Al-4V ELI samples show a distinct shift in the peak position which is commonly indicative of internal stress of a material. The intensity of the (100) peak was significantly reduced for both the 3D-Ti64 samples in comparison with the bulk-Ti64 sample.

4.1.2 White Light Interferometry (WLI) Measurement

We used a Bruker-AXS NT-9800 optical surface profiler with a 0.80 numerical aperture and 5x Michelson objective to measure the surface roughness and map the topography of our samples. We employed a VSI method to obtain the vertical height profile of the surfaces. The arithmetic average (R_a) surface roughness of each sample over a representative sample of 233 x 211 µm is presented in Table 7.

Table 7 Surface Roughness of Test Samples

TEST MATERIAL	SURFACE ROUGHNESS (R_a)
Bulk-Ti64	9.14×10^{-2} µm
FAD-Ti64	1.42×10^{-3} µm
3D-Ti64 (H)	2.85 µm
3D-Ti64 (V)	23.76 µm
DLC-Ti64 (H)	2.13 µm
DLC-Ti64 (V)	25.1 µm

The bulk and FAD Ti-6Al-4V samples had a significantly lower surface roughness than each of the EBM manufactured samples, with the FAD-Ti64 sample having a low surface roughness due to the polished silicon wafer substrate underneath. The EBM manufactured samples built in the horizontal orientation had a better surface finish than the vertical orientation samples, however, both were significantly rougher than the polished bulk material. The DLC coatings did not significantly change the surface roughness which indicates that the coating is topographically conformal.

4.1.3 Scanning Electron Microscopy (SEM) Imaging

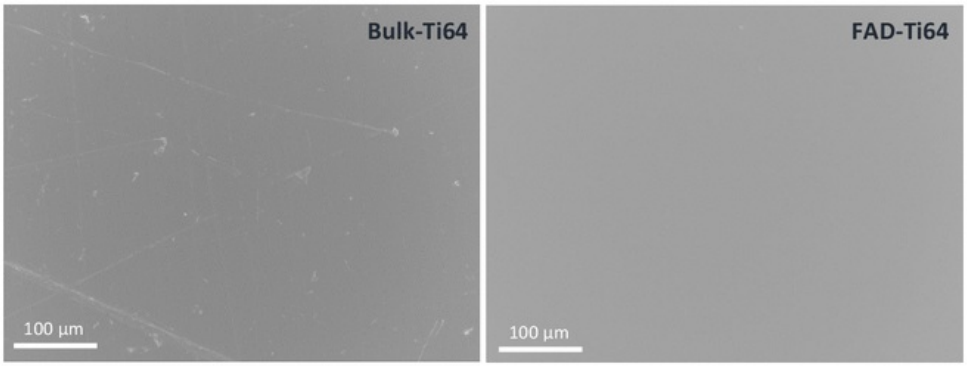

Figure 15 Left: SEM Image of Bulk-Ti64 Sample at 200x. Right: SEM Image of FAD-Ti64 Sample at 200x

The SEM images presented in Figure 15 indicate that both the bulk and FAD Ti-6Al-4V surface contain almost no surface features, and are smooth surfaces. The results from the WLI measurements conducted confirm that both samples have a low surface roughness (R_a) value.

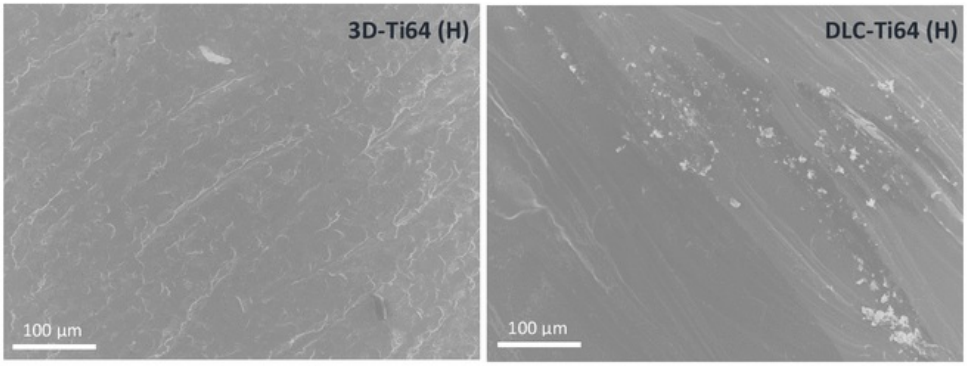

Figure 16 Left: SEM Image of 3D-Ti64 (H) Sample at 200x. Right: SEM Image of DLC-Ti64 (H) Sample at 200x

The SEM images presented in Figure 16 indicate that the DLC coating is conformal and does not significantly change the surface topography of the EBM manufactured materials. In the image on the left in Figure 16, it can be seen that the EBM manufactured surface contains smooth directional features where the powdered particles have been melted together by the electron beam.

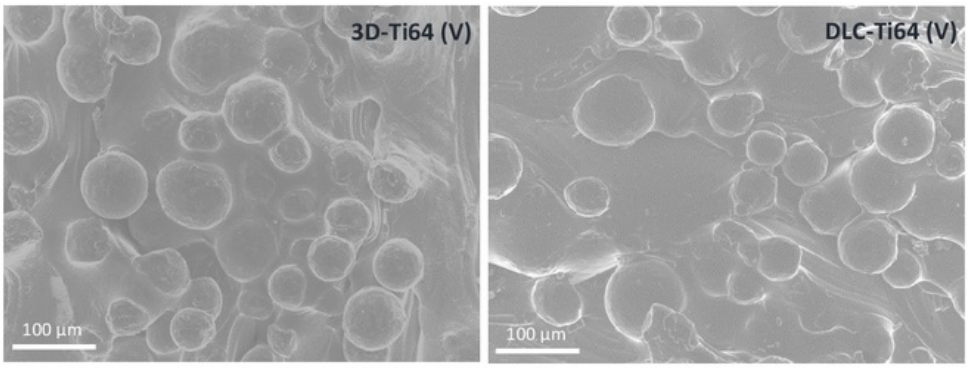

Figure 17 Left: SEM Image of 3D-Ti64 (V) Sample at 200x. Right: SEM Image of DLC-Ti64 (V) Sample at 200x

The SEM images presented in Figure 17 also confirm that the DLC coating is conformal and does not significantly alter the surface roughness. In Figure 17 Left it can be seen that unmelted particles form on the surface of the material when EBM manufactured in the vertical direction. The unmelted particles have a significant effect on the surface roughness of the material. This was also confirmed by the WLI surface roughness (R_a) measurements.

4.1.4 Energy Dispersive X-Ray (EDX) Spectroscopy

Table 8 Chemical Composition (in wt. %) of Samples with EDX Analysis

TEST MATERIAL	C (wt. %)	O (wt. %)	Al (wt. %)	Si (wt. %)	Ti (wt. %)	V (wt. %)
Bulk-Ti64	1.8	4.8	4.3	-	84.6	4.5
FAD-Ti64	-	-	2.7	6.6	86.8	3.9
3D-Ti64 (H)	2.3	-	5.4	-	88.6	3.7
3D-Ti64 (V)	1.7	-	4.2	-	89.8	4.3
DLC-Ti64 (H)	69.6	-	1.6	7.1	20.8	0.9
DLC-Ti64 (V)	60.8	-	1.6	4.8	31.5	1.3

The EDX analysis is conducted over a detection depth of approximately 1 µm and is considered to be representative of the bulk material. Our quantitative elemental composition results were calculated using the Oxford Instruments *AZtecEnergy* software package. We selected a representative region on our samples and conducted a spectral analysis at four points on the sample. The results obtained in Table 8 were the averaged values from the four sites that we analysed.

The EDX composition analysis indicated that all four of our samples contained a lower aluminium and vanadium content (in wt. %) than the minimum specifications of the material grade. It can also be seen that the EBM manufactured materials contained a slightly higher titanium content than the bulk and FAD samples.

The DLC-Ti64 samples contained a predominantly carbon and titanium at the bulk level. Small amounts of silicon were found as a result of the thin intermediate layer of amorphous silicon hydrogenated carbide (a:SiCH) that was deposited on the material substrate prior to the deposition of the final DLC layer. The FAD-Ti64 sample also contained small amounts of silicon, which indicates that the EDX analysis was able to detect the silicon wafer substrate underneath the Ti-6Al-4V coating.

4.1.5 X-Ray Photoelectron Spectroscopy (XPS)

Spectra presented in Figure 18 and Figure 19 have been vertically shifted by an arbitrary value for visual representation purposes.

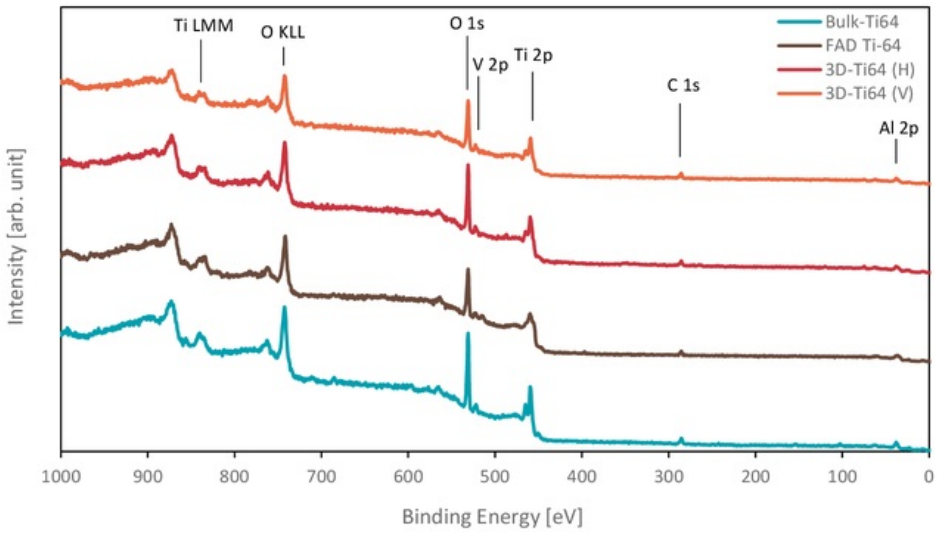

Figure 18 XPS Spectra of Uncoated Samples

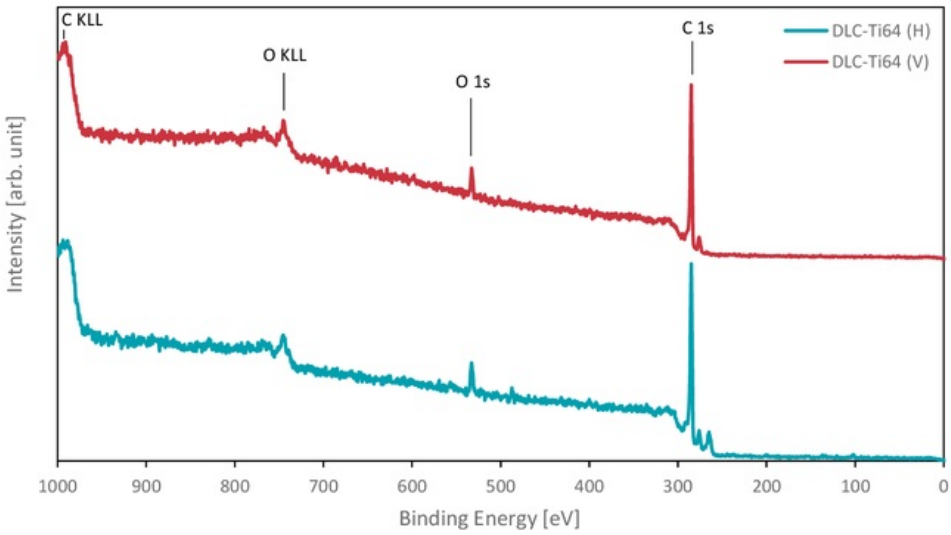

Figure 19 XPS Spectra of DLC Coated Samples

Table 9 Chemical Composition (in wt. %) of Samples with XPS Analysis

TEST MATERIAL	C (wt. %)	O (wt. %)	Al (wt. %)	Ti (wt. %)	V (wt. %)
Bulk-Ti64	8.62	42.8	3.00	43.3	2.28
FAD-Ti64	6.55	41.2	2.87	47.0	2.38
3D-Ti64 (H)	6.56	40.6	7.31	44.0	1.53
3D-Ti64 (V)	7.83	41.0	5.66	44.4	1.11
DLC-Ti64 (H)	90.1	7.59	1.08	0.38	0.85
DLC-Ti64 (V)	90.2	6.93	0.87	0.77	1.23

The XPS analysis is conducted over a detection depth of approximately 5 nm and is considered to be representative of the surface of the material. Our quantitative elemental composition results were calculated using the SPECS *SpecsLab* software package. We conducted a spectral analysis to characterise the intensity peaks as shown in shown in Figure 18 and Figure 19. From the XPS spectrums, we were able to calculate an approximate elemental composition for each sample as shown in Table 9.

The XPS composition analysis indicated that all Ti-6Al-4V samples contained a low vanadium content on the surface of the material, in comparison with the EDX results. The aluminium content for the 3D-Ti64 samples was significantly higher than both the Bulk-Ti64 and FAD-Ti64 samples. The carbon and oxygen content of the surface has also increased as expected due to environmental contaminations and the reactivity titanium oxides on the surface. The titanium content has been significantly reduced, as a result.

The DLC coated Ti-6Al-4V ELI samples contained a high carbon content with a small percentage of oxygen present, which was as expected. Trace amounts of titanium, aluminium and vanadium indicate that our material was completely coated in DLC.

4.1.6 Low Energy Ion Scattering (LEIS) Spectroscopy

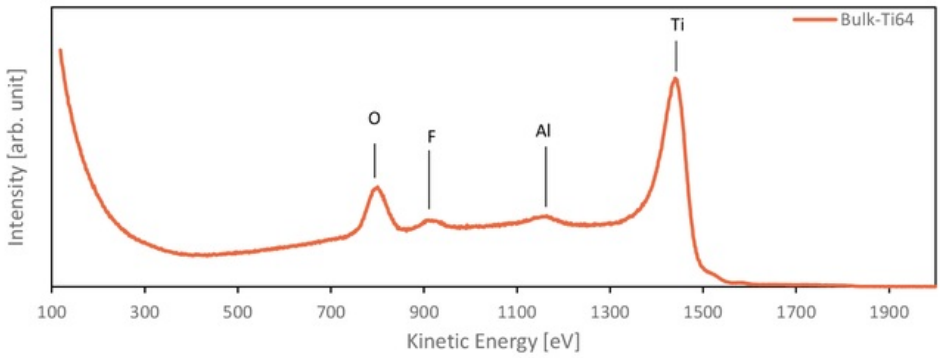

Figure 20 LEIS Spectra of Bulk-Ti64 Sample

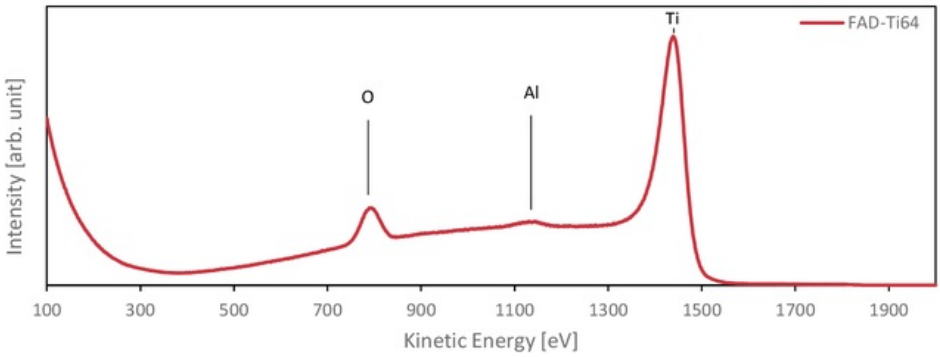

Figure 21 LEIS Spectra of FAD-Ti64 Sample

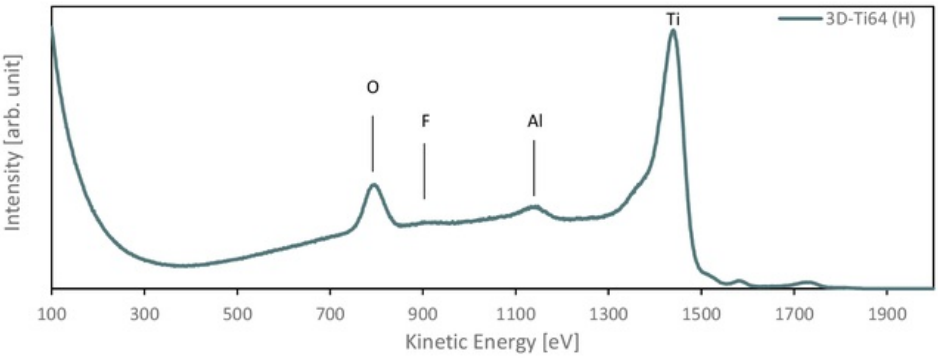

Figure 22 LEIS Spectra of 3D-Ti64 (H) Sample

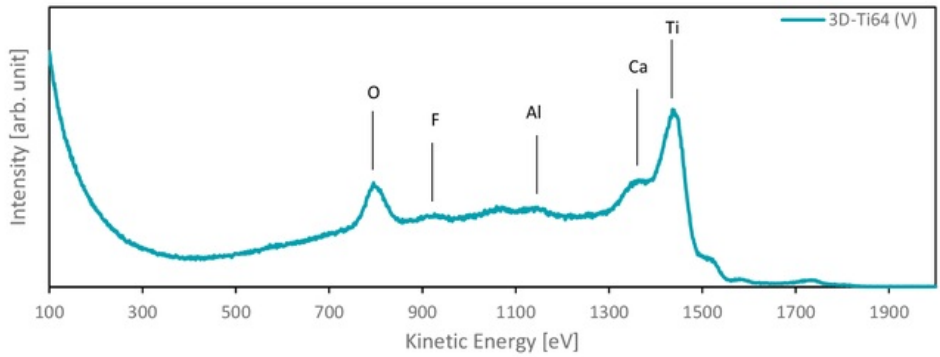

Figure 23 LEIS Spectra of 3D-Ti64 (V) Sample

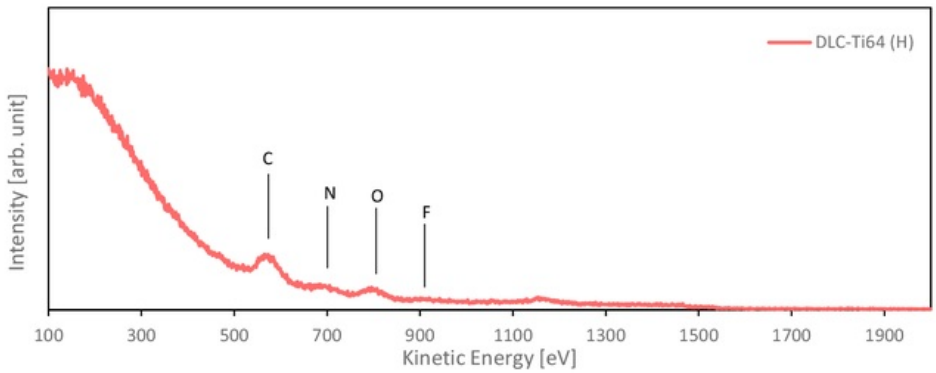

Figure 24 LEIS Spectra of DLC-Ti64 (H) Sample

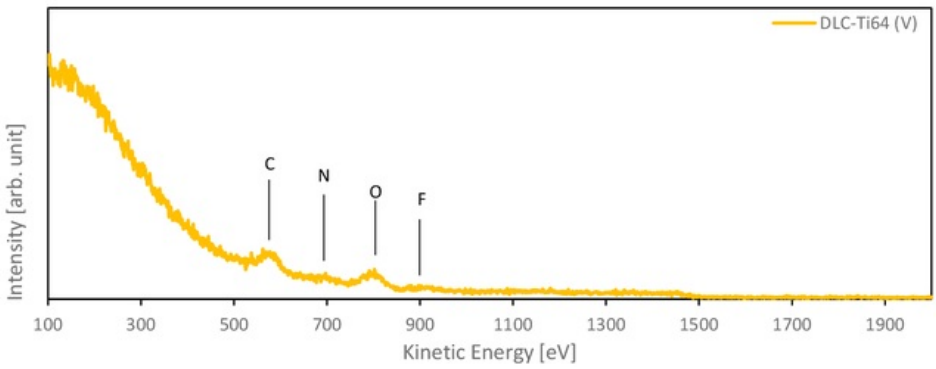

Figure 25 LEIS Spectra of DLC-Ti64 (V) Sample

Table 10 Chemical Composition (in wt. %) of Samples with LEIS Analysis

TEST MATERIAL	C (wt. %)	N (wt. %)	O (wt. %)	F (wt. %)	Al (wt. %)	Ca (wt. %)	Ti (wt. %)
Bulk-Ti64	-	-	24.7	3.8	3.1	-	68.3
FAD-Ti64	-	-	16.6	-	1.7	-	81.7
3D-Ti64 (H)	-	-	20.4	0.9	4.9	-	73.9
3D-Ti64 (V)	-	-	31.3	3.4	5.7	2.6	57.0
DLC-Ti64 (H)	67.8	12.7	16.1	3.4	-	-	-
DLC-Ti64 (V)	51.9	12.2	29.6	6.3	-	-	-

The LEIS analysis is conducted over a detection depth of approximately the first atomic layers and is considered to be representative of the outermost surface of the material. Our quantitative elemental composition results were calculated using the SPECS *SpecsLab* software package. We selected a representative region on each sample and conducted a spectral analysis to characterise the intensity peaks as shown in Figure 20 to Figure 25. We used a calibration curve to determine the peak positions on the spectra to identify the elements associated with that peak. We calculated the approximate composition of the surface by correcting the intensity of the final energy of the ion for the differences in atomic radii of the surface elements, in the same method as presented by Ackermans [51]. The approximate elemental composition was calculated in atomic percent and then converted into weight percent by accounting for the atomic weight of each element. The results are presented in Table 10.

There was no vanadium present in the outer atomic layers of any of our samples, whilst the aluminium content was consistent with the XPS results for the same samples. The titanium content increased for all Ti-6Al-4V samples. However, the oxygen content for all the Ti-6Al-4V samples had decreased at the surface of the material in comparison with the XPS results. Trace amounts of fluorine were found to be present in all of our samples and are due to contamination from one the O-rings inside the LEIS vacuum chamber.

The DLC-Ti64 samples contained a lower carbon content in the outer atomic layers, as there was an increase in the oxygen content as expected due to the reactivity of surface oxides. Nitrogen contamination occurred during the PACVD process and was found in small quantities only in the outermost atomic layers. Fluorine was also found to be present on the surface of the material, which can be attributed to contaminants during the LEIS analysis.

4.1.7 Surface Wettability

The surface wettability was determined by contact angle measurements with a 5 µL droplet of water at room temperature. Contact angle measurements were taken by analysing photographic images with the open-source program *ImageJ*. The contact angle measurements are shown in Figure 26:

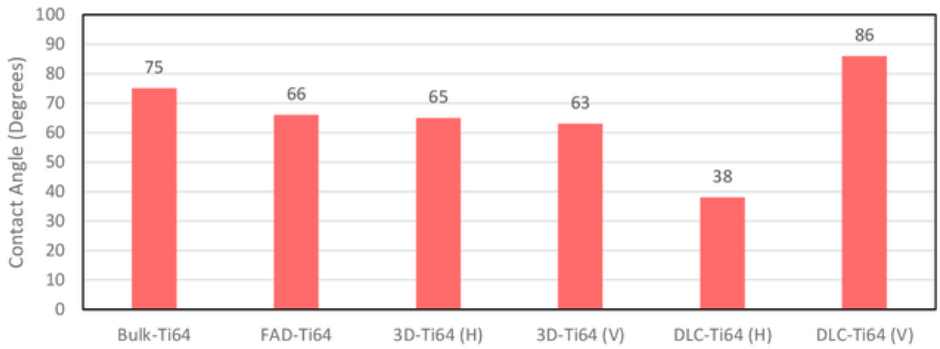

Figure 26 Contact Angle Measurements of Test Samples

All test samples were hydrophilic, with the both the 3D-Ti64 and the FAD-Ti64 samples having an approximately equal surface wettability. The DLC coatings had significantly different contact angles, with the DLC-Ti64 (H) having the lowest contact angle which implies that this surface was more wettable than any other surface. In contrast, the DLC-Ti64 (V) sample was the least wettable surface.

4.2 Biological Testing of Materials

4.2.1 Indirect Cytotoxicity Assay

Extracts of samples that were collected were not tested in an indirect cytotoxicity assay for two reasons. Firstly, the preliminary work study showed that there were only marginal toxicity issues with these EBM manufactured surface. Secondly, imaging of cells around samples in 7-day proliferation assay revealed normal cell morphology at all time-points. Taken together, there was no need to perform a cytotoxicity test.

4.2.2 Cell Adhesion and Proliferation Assay

All samples showed cell attachment and spreading after 24 h, and continued to spread after 48 h. At the 48 h time point, the number of cells which had started to spread had increased. In order for visualisation of cell morphology with microscopy, the actin cytoskeletons on cells are tagged using a phalloidin stain (which appear in red), and cell nuclei are tagged using a DAPI ($C_{16}H_{17}Cl_2N_5$) stain (which appear in blue)

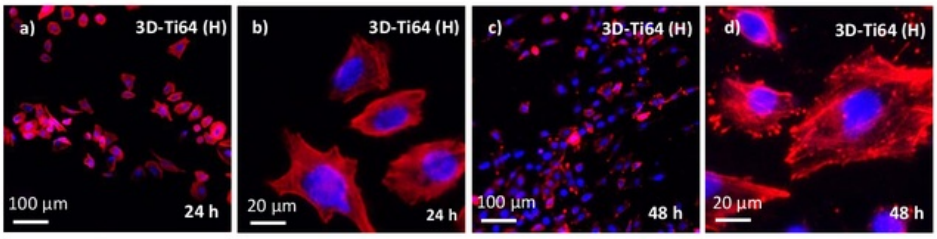

Figure 27 Representative Fluorescent Images of Phalloidin (Red) and DAPI (Blue) Stained Cells. a) 3D-Ti64 (H) after 24 h at 20x. b) 3D-Ti64 (H) after 24 h at 100x. c) 3D-Ti64 (H) after 48 h at 20x. d) 3D-Ti64 (H) after 48 h at 100x.

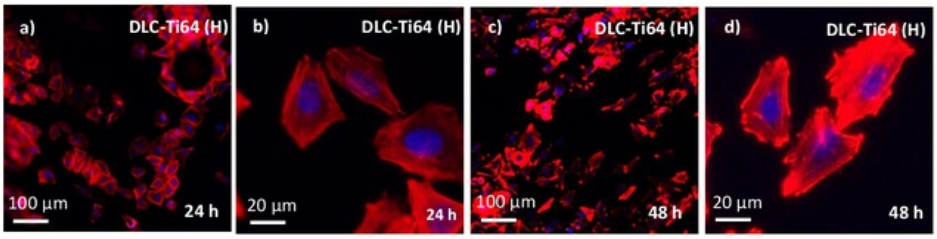

Figure 28 Representative Fluorescent Images of Phalloidin (Red) and DAPI (Blue) Stained Cells. a) DLC-Ti64 (H) after 24 h at 20x. b) DLC-Ti64 (H) after 24 h at 20x. c) DLC-Ti64 (H) after 48 h at 20x. d) DLC-Ti64 (H) after 48 h at 100x.

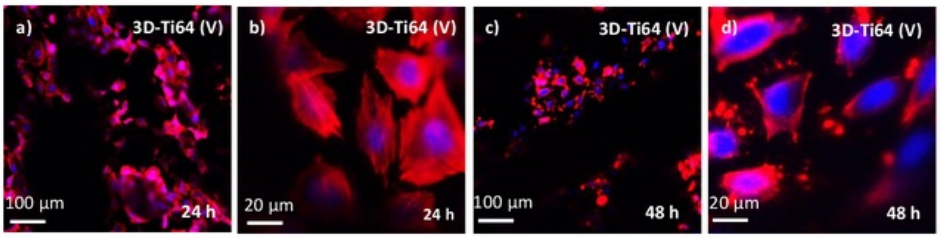

Figure 29 Representative Fluorescent Images of Phalloidin (Red) and DAPI (Blue) Stained Cells. a) 3D-Ti64 (V) after 24 h at 20x. b) 3D-Ti64 (V) after 24 h at 100x. c) 3D-Ti64 (V) after 48 h at 20x. d) 3D-Ti64 (V) after 48 h at 100x.

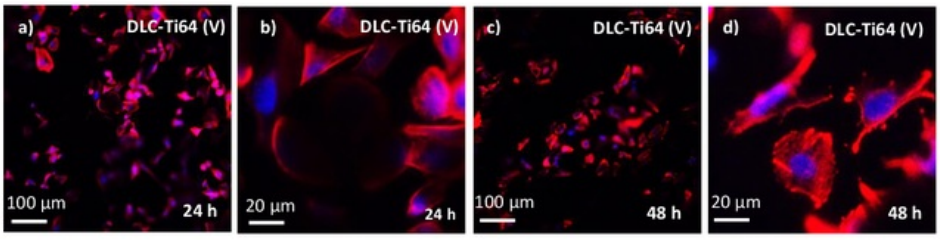

Figure 30 Representative Fluorescent Images of Phalloidin (Red) and DAPI (Blue) Stained Cells. a) DLC-Ti64 (V) after 24 h at 20x. b) DLC-Ti64 (V) after 24 h at 100x. c) DLC-Ti64 (V) after 48 h at 20x. d) DLC-Ti64 (V) after 48 h at 100x.

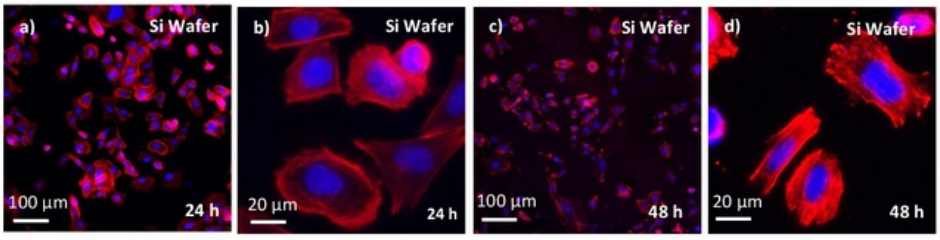

Figure 31 Representative Fluorescent Images of Phalloidin (Red) and DAPI (Blue) Stained Cells. a) Si Wafer after 24 h at 20x. b) Si Wafer after 24 h at 100x. c) Si Wafer after 48 h at 20x. d) Si Wafer after 48 h at 100x.

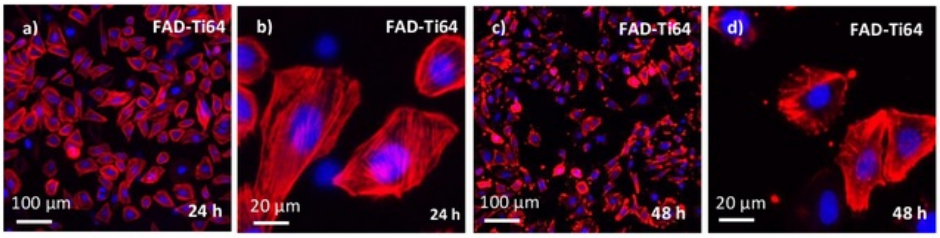

Figure 32 Representative Fluorescent Images of Phalloidin (Red) and DAPI (Blue) Stained Cells. a) FAD-Ti64 after 24 h at 20x. b) FAD-Ti64 after 24 h at 100x. c) FAD-Ti64 after 48 h at 20x. d) FAD-Ti64 after 48 h at 100x.

Cells on the 3D-Ti64 (H), DLC-Ti64 (H) and DLC-Ti64 (V) surfaces were more evenly spread than cells adherent to the 3D-Ti64 (V) sample. This suggests that surface chemistry and morphology of the EBM manufactured samples affected cell growth. This is further confirmed by cell response of the Si wafer and FAD-Ti64 samples, as these samples had attachment and spread with well-defined actin cytoskeletons at both the 24 h and 48 h time points.

Cell proliferation measures the increase in the number of cells over a period of time. The data presented in Figure 33 represents the mean value of cells adherent to the surface of each sample calculated from triplicate wells of each sample at each time-point, adjusted to take into account the difference in area between to the test samples and TCPS control wells so they can be compared using the optical density readings at a wavelength of 595 nm/cm^2.

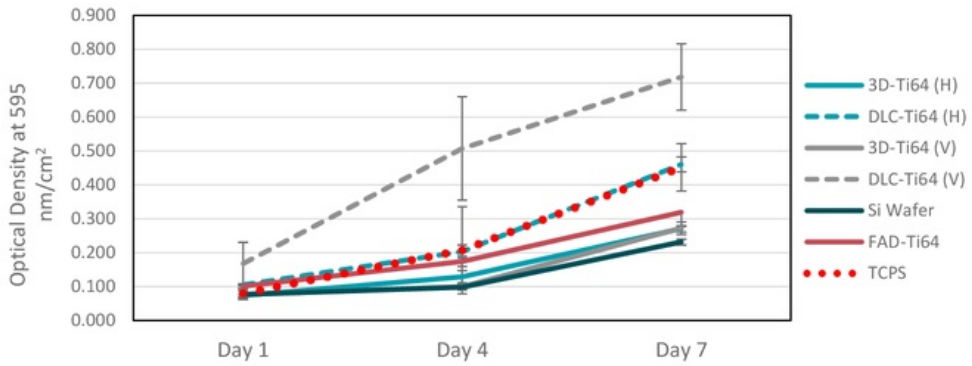

Figure 33 7-Day Proliferation Assay Results of Test Samples

The outcomes from the cell proliferation assay indicated that the DLC-Ti64 (V) sample supported the superior proliferation of cells as compared with all other materials including TCPS which served as our positive control. The proliferation of cells on the DLC-Ti64 (H) samples was less than that of the DLC-Ti64 (V) samples however the surface performed equally as well as the TCPS control. The most notable difference in proliferation occurred on Day 7, were all other samples performed similarly and were all less than the TCPS control. These results indicated that the DLC coating of the EBM manufactured Ti-6Al-4V ELI samples promoted greater rates of cell proliferation than the uncoated materials at every time-point in the assay.

4.2.3 Cell Differentiation and Mineralisation Assay

Alkaline phosphatase (ALP) is regarded as an early marker of cell differentiation, and we measured the amount of ALP that was produced at the end of the 23-day assay. The data presented in Figure 34 represents the mean value of triplicate samples for each material, normalised to the value for the TCPS control in osteogenic medium and adjusted for the number of cells attached to each surface as determined by MTT assay which was run in parallel with the differentiation assay.

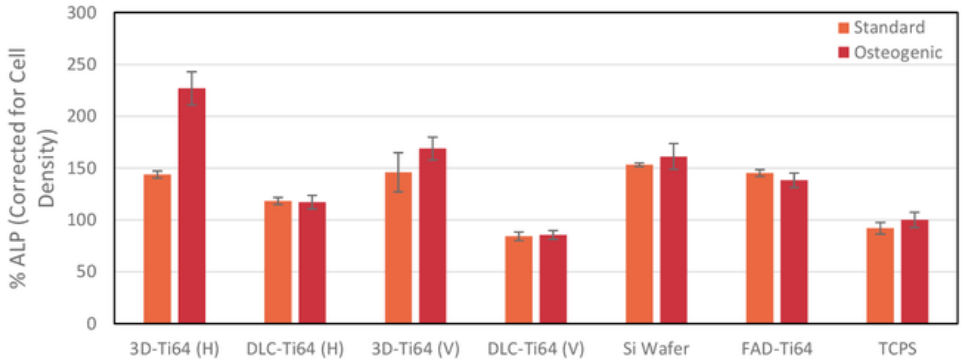

Figure 34 Alkaline Phosphatase (ALP) Production of Cells on Day 23

The outcomes presented in Figure 34 indicated that cells on all test surfaces except for the DLC-Ti64 (V) sample produced ALP levels that were higher than the TCPS control under both standard and osteogenic culture conditions. The DLC-Ti64 (H) and DLC-Ti64 (V) samples produced less ALP than the uncoated 3D-Ti64 (H) and 3D-Ti64 (V) samples, which indicates that these cells were not in the earlier stages of differentiation under either culture conditions.

The culture conditions did not make much difference to the amount of ALP produced on any surfaces except on 3D-Ti64 (H) which supported significantly higher levels of ALP when cells were maintained under osteogenic conditions indicating that these cells were active in the earlier stage of cell differentiation at day 23.

Calcium production by the adherent cells is a marker of the later phase of cell differentiation involving the mineralisation of the extracellular matrix produced by the cells as they start to form bone. The data presented in Figure 35 represents the mean value of triplicate samples for each material, normalised to the value for the TCPS control in osteogenic medium and adjusted for the number of

cells attached to each surface as determined by MTT assay which was run in parallel with the differentiation assay.

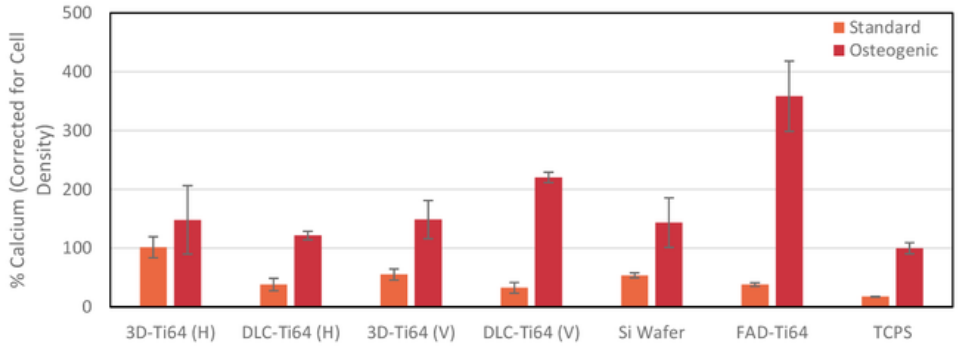

Figure 35 Calcium Production of Cells on Day 23

The outcomes presented in Figure 35 indicate that cells on all test surfaces including the TCPS control produced significantly more calcium when maintained under osteogenic culture conditions compared with standard conditions. Cells on the FAD-Ti64 sample produced significantly higher levels of calcium per cell than all other surfaces. The DLC-Ti64 (V) samples had greater levels of calcium production than all other EBM manufactured materials 3D-Ti64 (H), 3D-Ti64 (V) or the DLC-Ti64 (H) sample which all produced approximately equivalent levels of calcium.

5. Discussion

5.1 Thin Film Material Deposition

DLC coatings were successfully applied to both the 3D-Ti64 substrates using a PACVD process. This was confirmed by the SEM images in Figure 16 and Figure 17 that show that the DLC coating was conformal as the surface topography is not significantly altered by the deposition of the DLC coating. Visual observations also support that the inference that the coating is conformal as surface features are consistently present on both the coated and uncoated samples. The coated and uncoated samples are shown in Figure 36.

Figure 36 DLC Coated and Uncoated 3D-Ti64 Test Samples

The PACVD deposition process is conformal as the DLC film is produced from the growth of the nucleation of reactant species which form on the surface in a line of sight manner. This causes the film to encase the entire surface of the substrate, including all surface undulations.

The WLI results also indicated that the surface roughness was almost identical between the DLC coated and uncoated materials, which further indicates that the coating was indeed conformal. Additional LEIS results (as presented in Table 10) confirm that the material was completely coated in DLC as the elemental composition contained only trace amounts of titanium, vanadium or aluminium in the outermost atomic layers of the material.

5.2 Characterisation of Materials

In order to confirm that the 3D-Ti64 materials were of the same bulk crystalline structure as our commercially produced Bulk-Ti64 sample, we conducted X-Ray Diffraction (XRD) analysis. The XRD patterns indicated that the observed peaks of the Bulk-Ti64 samples were also present in the XRD patterns of the 3D-Ti64 samples, which were consistent with peak positions observed in the literature [65, 66]. However, both 3D-Ti64 samples were slightly up-shifted from the reference peak positions of our Bulk-Ti64 XRD pattern. The shift in the peak position for the 3D-Ti64 materials suggests that there exists residual stress in the EBM parts as a result of the manufacturing process. A study by Kok *et al.* [67] observed similar shifting of the peak positions and has also suggested that it could be due to residual stress in EBM manufactured parts.

The surface roughness of our EBM manufactured materials was measured using WLI in order to compare the surface topography of the 3D-Ti64 (H) and 3D-Ti64 (V) samples. The results presented in Table 7 indicated that the 3D-Ti64 (H) sample has a reduced surface roughness when compared with the 3D-Ti64 (V) sample, which suggests that further optimisation of the build orientation should be considered when using EBM manufacturing. These results confirmed visual observations that as-built EBM manufactured parts have significantly greater surface roughness than commercially produced and polished Ti-6Al-4V samples. Studies by Klingvall *et al.* [68] and Safdar *et al.* [69] have suggested that the EBM process parameter settings can have a significant effect on the surface roughness of manufactured parts, and should be considered when engineering micro-architecture for biomaterials.

The EDX results also confirmed that the elemental composition of the Bulk-Ti64 material is comparable with the 3D-Ti64 samples at the bulk material level. This suggests that the cell response to the materials is not due to any differences in the bulk material, as our EBM parts have the same bulk structure as our reference bulk Ti-6Al-4V sample. The EDX elemental quantifications indicated that both the Bulk-Ti64 and both 3D-Ti64 materials contained a lower aluminium and vanadium content (in wt. %) than the minimum specifications of the material grade.

However, the XPS results indicated that the aluminium content of the Bulk-Ti64 material was reduced at the surface of the material. This result was not observed in the 3D-Ti64 materials as the aluminium content actually increased at the surface of the material. There was a reduced vanadium content at the surface of the material at the XPS detection depth. This trend indicates that the vanadium content of all our materials decreases as you move closer to the surface of the material. The lack of vanadium on the surface of Ti-6Al-4V materials is well documented in the literature [70, 71]. The LEIS elemental

quantifications indicated that there was no vanadium atoms present on the surface of any of our test materials, however, the aluminium content was consistent with the XPS results.

The contact angle measurements of all the surfaces except for DLC-Ti64 (V) indicated that all surfaces were moderately hydrophilic, with the exception of the DLC-Ti64 (H) sample which was only marginally hydrophilic. However, due to the extreme surface roughness of 3D-Ti64 samples, the reliability and validity of this result could be further improved by using the Wenzel equation instead of the Young equation used in our results. The FAD-Ti64, 3D-Ti64 (H) and 3D-Ti64 (V) had approximately equal contact angle measurements, and the Bulk-Ti64 sample was more hydrophilic than all other Ti-6Al-4V materials.

5.3 Biological Testing of Materials

5.3.1 Cell Adhesion and Proliferation

The data from the short-term assays showed that all of the surfaces supported cell adhesion in the first 24-48 h of culture. Cells on the 3D-Ti64 (H), DLC-Ti64 (H) and DLC-Ti64 (V) surfaces were more evenly spread than cells adherent to the 3D-Ti64 (V) sample. This suggests that both surface chemistry and morphology have an effect on the cellular response of Saos-2 cells. This is further confirmed by cell response of the Si wafer and FAD-Ti64 samples, as these samples had attachment and spread with well-defined actin cytoskeletons at both the 24 h and 48 h time points. Cell morphology of each sample is shown in Figure 37 to Figure 39. All cells showed evidence of spreading out after 24 h in culture, which indicates that all the surfaces support cell proliferation.

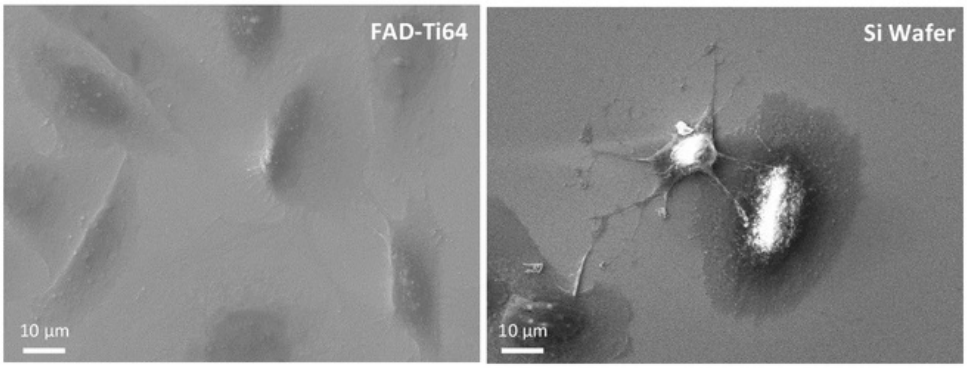

Figure 37 Left: SEM Image of Cell Morphology after 24 h on FAD-Ti64 Sample. Right: SEM Image of Cell Morphology after 24 h on Si Wafer Sample.

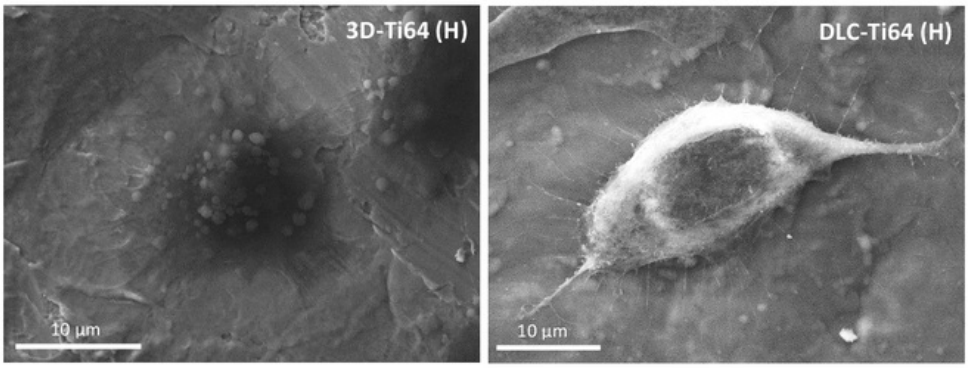

Figure 38 Left: SEM Image of Cell Morphology after 24 h on 3D-Ti64 (H) Sample. Right: SEM Image of Cell Morphology after 24 h on DLC-Ti64 (H) Sample.

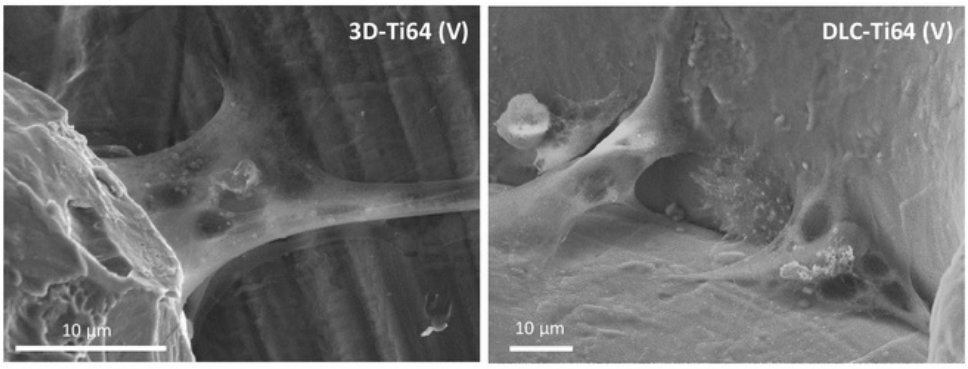

Figure 39 Left: SEM Image of Cell Morphology after 24 h on 3D-Ti64 (V) Sample. Right: SEM Image of Cell Morphology after 24 h on DLC-Ti64 (V) Sample.

Cells on the 3D-Ti64 (H) and DLC-Ti64 (H) samples contained a similar morphology to the FAD-Ti64 and Si wafer samples, whilst cells on the 3D-Ti64 (V) and DLC-Ti64 (V) had a completely different morphology. The DLC-Ti64 samples contained cells which had developed extensive filopodia which indicate that the cells are spreading more actively on these surfaces as compared the 3D-Ti64 surfaces. This could explain why the rate of proliferation was much greater on the DLC-Ti64 surfaces.

In the 3D-Ti64 (V) and DLC-Ti64 (V) samples, the cells attached formed bridge-like structures between the valleys and the unmelted particles on the surface of the material. These bridge-like structures can be attributed to a low energy output/input expenditure from the cell which is favourable for cell attachment. A similar behaviour was reported in a study by Ponader *et al.* [72], where hFOB 1.19 human foetal osteoblasts also formed in low-lying areas around unmelted particles. This suggests that the both the surface morphology and the chemistry of the DLC-Ti64 (V) samples provides an optimal environment for cell proliferation.

There is no general agreement that either smooth or rough surfaces enhance cell attachment or proliferation, however, surfaces at either extreme are generally considered to not enhance the cell response [72]. This could explain that due to a reduced surface roughness, the FAD-Ti64 samples had a greater rate of cell proliferation than both 3D-Ti64 samples which were excessively rough. However, the FAD-Ti64 sample still had a lower rate of proliferation than both DLC-Ti64 samples which further suggests that cells found the surface chemistry of DLC more favourable than Ti-6Al-4V.

The Si wafer, FAD-Ti64 and TCPS control samples all had an even distribution of cells across the surface, however, the Si wafer samples had a significantly lower rate of proliferation than the FAD-Ti64 and the TCPS control. This confirms that the Ti-6Al-4V material is influencing the cell response.

Images of adherent cells on all surfaces stained with CTG showed good cell coverage over the longer 23-day assay which was run in parallel to account for cell numbers on each material. All materials contained cell numbers that were at least equivalent to the TCPS control, which suggests that all materials were supporting cell proliferation.

In contrast, the cells adherent to the 3D-Ti64 (V) and DLC-Ti64 (V) samples formed in 'crater-like' clusters which are indicative of the surface topographical features in which the cells are unable to cover. From SEM imaging of these cells, it is clear that the cells (seen as black dots in the image on the left) did not adhere on top of the unmelted particles which are present on the 3D-Ti64 (V) surface as shown in Figure 40. This is supported by the CTG images of the cells on day 23, where cells did grow in certain regions, resulting in the black 'crater-like' features as shown in Figure 40. The behaviour of cells to favourably attach to the deep-lying areas between the higher peaks of the unmelted particles is attributed to a lower energy expenditure/input [72].

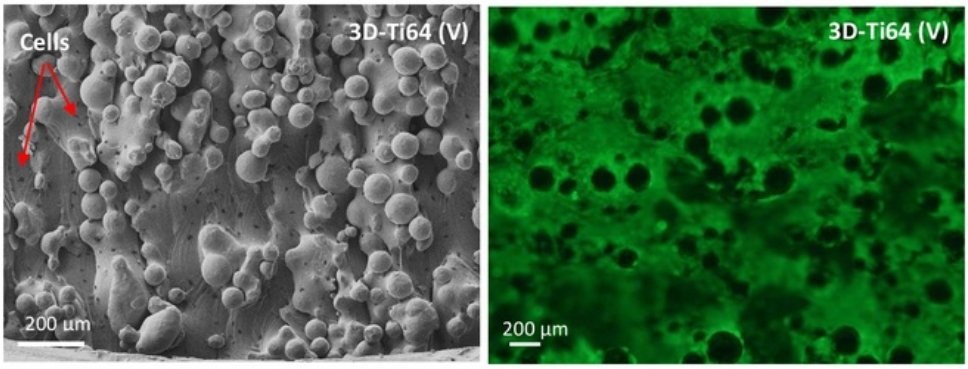

Figure 40 Left: SEM Image of EBM Manufactured Ti-6Al-4V ELI (Vertically Built) with Cells after 24 h. Right: CTG Staining Images of EBM Manufactured Ti-6Al-4V ELI (Vertically Built) on Day 23

The Si wafer, FAD-Ti64 and TCPS control samples did not show any evidence of cell patterning and instead formed evenly across the surface of the material. The Si wafer sample had the least cell coverage after 23 days, which suggests that the cells found this surface to be least favourable.

5.3.2 Cell Differentiation and Mineralisation Assay

As bone-forming cells mature/differentiate they produce calcium phosphate crystals in a biological process known as mineralisation. This can be measured *in vitro* using Saos-2 cells and assessing the differentiation and mineralisation of cells adherent to a substrate over a period of 23 days.

The outcomes from the mineralisation assay indicated that all surfaces except for 3D-Ti64 (V) produced ALP levels that were higher than the TCPS control. The DLC coated materials produced less ALP than the uncoated EBM manufactured samples which indicated that these cells were not in the earlier stages of differentiation under either culture conditions. The expectation is that this is because these surfaces produced more calcium indicating that the cells were in a later stage of differentiation and starting to mineralise their extracellular matrix. This was true for the DLC-Ti64 (V) samples, however, it was not the case for the DLC-Ti64 (H) sample. Cells on the DLC-Ti64 (V) surface maintained under osteogenic conditions were in a more advanced state of differentiation than the other surfaces, as evidenced by calcium production which is indicative of the mineralisation process having been commenced. Whilst cells on all surfaces were able to differentiate to at least some extent as measured by the ALP and calcium production (as shown in Figure 34 and Figure 35).

6. Conclusions

DLC coatings can be successfully deposited onto to both horizontally and vertically built Ti-6Al-4V ELI alloy materials that have been manufactured by EBM technology. These materials were fully characterised with respect to the chemical and physical properties. Biological testing of these materials using the Saos-2 cell line confirmed our hypothesis that DLC coatings were shown to have a positive effect on the rate of cell proliferation.

However, an overall improved cell response is was not found to be conclusively a result of the DLC coating, as there are additional underlying effects such as build orientation and surface morphology that was previously unknown. It is believed that the extreme surface roughness of the as-built EBM materials had a significant effect on the reliability of our results.

The XRD analysis also indicated that there exists residual stress in the EBM parts, which is not present in the commercially produced bulk material sample. This is of a concern because residual stresses in the material can lead to premature failure of the part.

7. Recommendations for Future Work

At present, a comprehensive literature and background theory review has been conducted to determine the current state-of-the-art technology. A full set of biological tests and surface characterisation analyses were designed to ensure that an in-depth understanding of each of the sample materials could be reached. Future work will enable the elucidation between the benefits of DLC coatings and the contribution to the cell proliferation behaviour for osseointegration.

Due to the complicated nature of biological testing, future work could be concerned with expanding this research with different cell models or conducting *in vivo* testing. This would allow for a more reliable set of results that could further investigate the successfulness of DLC coatings for additive manufactured materials. Additional research could also be concerned with doped DLC coatings that have been engineering to further enhance the cell response.

Future work could also be concerned with the development of etching techniques that can alter the surface energy of a material, whilst maintain the morphology of the surface. As on the major issues with EBM manufacturing is the poor surface finish of the build part, etching techniques could also provide a solution to intensive post-processing polishing techniques.

8. Abbreviations

AM	Additive Manufacturing
ASME	American Society of Mechanical Engineers
ASTM	American Society for Testing and Materials International
BCC	Body-Centred Cubic
CAD	Computer Aided Design
DLC	Diamond-like Carbon
DMLS	Direct Metal Laser Sintering
EBM	Electron Beam Melting
EDX	Energy Dispersive X-Ray Spectroscopy
FAD	Filtered Arc Deposition
FDA	The United States Food and Drug Administration
HCP	Hexagonal Close Packed
HRC	Rockwell Hardness C
ISO	International Standards Organisation
LEIS	Low Energy Ion Scattering
MTT	Microculture Tetrazolium
NIH	United States National Institute of Health
PACVD	Plasma Activated Chemical Vapour Deposition
PBF	Powder Bed Fusion
SEM	Scanning Electron Microscopy
SFM	Serum-Free Medium
SLM	Selective Laser Melting
SLS	Selective Laser Sintering
STL	Standard Tessellation Language or Stereolithography Interface Format
TCPS	Tissue Culture Polystyrene
UTS	Ultimate Tensile Strength
WLI	White Light Interferometry
XPS	X-Ray Photoelectron Spectroscopy
XRD	X-Ray Diffraction
YS	Yield Strength

References

[1] V. Sansone, D. Pagani, and M. Melato, "The effects on bone cells of metal ions released from orthopaedic implants. A review," *Clinical Cases in Mineral and Bone Metabolism,* vol. 10, pp. 34-40, Jan-Apr 2013.

[2] G. D. Revankar, R. Shetty, S. S. Rao, and V. N. Gaitonde, "Wear resistance enhancement of titanium alloy (Ti–6Al–4V) by ball burnishing process," *Journal of Materials Research and Technology,* 2016.

[3] M. J. Nine, D. Choudhury, A. C. Hee, R. Mootanah, and N. A. Abu Osman, "Wear Debris Characterization and Corresponding Biological Response: Artificial Hip and Knee Joints," *Materials,* vol. 7, pp. 980-1016, Feb 2014.

[4] B. Daley, A. T. Doherty, B. Fairman, and C. P. Case, "Wear debris from hip or knee replacements causes chromosomal damage in human cells in tissue culture," *Journal of Bone & Joint Surgery, British Volume,* vol. 86-B, p. 598, 2004.

[5] P. D. Lima, D. S. Leite, M. C. Vasconcellos, B. C. Cavalcanti, R. A. Santos, L. V. Costa-Lotufo*, et al.*, "Genotoxic effects of aluminum chloride in cultured human lymphocytes treated in different phases of cell cycle," *Food Chem Toxicol,* vol. 45, pp. 1154-9, Jul 2007.

[6] C. W. Lin, C. P. Ju, and J. H. Chern Lin, "A comparison of the fatigue behavior of cast Ti-7.5Mo with c.p. titanium, Ti-6Al-4V and Ti-13Nb-13Zr alloys," *Biomaterials,* vol. 26, pp. 2899-907, Jun 2005.

[7] ASTM F2792-12a, Standard Terminology for Additive Manufacturing Technologies (Withdrawn, 2015), ASTM International, West Conshohocken, PA, 2012, http://www.astm.org/cgi-bin/resolver.cgi?F2792

[8] I. Gibson, W. D. Rosen, and B. Stucker, "Introduction and Basic Principles," in *Additive Manufacturing Technologies: Rapid Prototyping to Direct Digital Manufacturing*, ed Boston, MA: Springer US, 2010, pp. 20-35.

[9] I. Gibson, W. D. Rosen, and B. Stucker, "Photopolymerization Processes," in *Additive Manufacturing Technologies: Rapid Prototyping to Direct Digital Manufacturing*, ed Boston, MA: Springer US, 2010, pp. 78-119.

[10] Commonwealth Scientific and Industrial Research Organisation, "Cancer patient receives 3D printed ribs in world first surgery," 11 September 2015. [Online] Available: http://www.csiro.au/en/News/News-releases/2015/Cancer-patient-receives-3D-printed-ribs-in-world-first-surgery. [Accessed 5 August 2016].

[11] Commonwealth Scientific and Industrial Research Organisation, "CSIRO produces 3D heel in world first surgery," 22 October 2014. [Online] Available: http://www.csiro.au/en/News/News-releases/2014/3D-Heel-In-World-First-Surgery. [Accessed 5 August 2016].

[12] Loughborough University, "About Additive Manufacturing," n.d. [Online] Available: http://www.lboro.ac.uk/research/amrg/about/the7categoriesofadditivemanufacturing/powderbedfusion/. [Accessed 18 July 2016].

[13] B. Dutta and F. H. Froes, "Chapter 3 - Additive Manufacturing Technology," in *Additive Manufacturing of Titanium Alloys*, ed: Butterworth-Heinemann, 2016, pp. 25-40.

[14] EOS GmbH, "Additive Manufacturing, Laser-Sintering and industrial 3D printing - Benefits and Functional Principle," n.d. [Online] Available: http://www.eos.info/additive_manufacturing/for_technology_interested. [Accessed 25 August 2016].

[15] Commonwealth Scientific and Industrial Research Organisation, "LaserCUSING metal 3D printer from Concept Laser," n.d. [Online] Available: https://research.csiro.au/metals/add-manufacturing/aus-innovation/lasercusing-germany/. [Accessed 25 August 2016].

[16] Arcam AB, "EBM Electron Beam Melting," n.d. [Online] Available: http://www.arcam.com/technology/electron-beam-melting/. [Accessed 26 April 2016].

[17] Kennametal, "Titanium Machining Guide," n.d. [Online] Available: https://www.kennametal.com/content/dam/kennametal/kennametal/common/Resources/Catalogs-Literature/Industry%20Solutions/Titanium_material_machining_guide_Aerospace.pdf. [Accessed 26 August 2016].

[18] I. Gibson, W. D. Rosen, and B. Stucker, "Powder Bed Fusion Processes," in *Additive Manufacturing Technologies: Rapid Prototyping to Direct Digital Manufacturing*, ed Boston, MA: Springer US, 2010, pp. 120-159.

[19] Arcam AB, "Arcam A1," n.d. [Online] Available: http://www.arcam.com/wp-content/uploads/Arcam-A1.pdf. [Accessed 18 August 2016].

[20] Concept Laser GmbH, "M2 cusing Multilaser Metal laser melting system," November 2014. [Online] Available: http://www.conceptlaserinc.com/wp-content/uploads/2014/11/M2cusingMultilaser_EN.pdf. [Accessed 18 August 2016].

[21] M. Koike, P. Greer, K. Owen, G. Lilly, L. E. Murr, S. M. Gaytan, *et al.*, "Evaluation of Titanium Alloys Fabricated Using Rapid Prototyping Technologies-Electron Beam Melting and Laser Beam Melting," *Materials,* vol. 4, pp. 1776-1792, Oct 2011.

[22] C. Henry, "CSIRO Metallic Additive Manufacturing High Performance Metal Program," presented at the Construction Materials Industry Conference, Brisbane, 2014.

[23] C. Engel. Selective Laser Melting versus Electron Beam Melting [Online]. Available: http://www.slideshare.net/carstenengel/selective-laser-melting-versus-electron-beam-melting

[24] L. Loeber, S. Biamino, U. Ackelid, S. Sabbadini, P. Epicoco, P. Fino, *et al.*, "Comparison of selective laser and electron beam melted titanium aluminides," in *Proceedings of the Solid Freeform Fabrication Symposium, Austin, TX, USA*, 2011, pp. 8-10.

[25] S. Rengers, "Electron Beam Melting [EBM] vs. Direct Metal Laser Sintering [DMLS]," 2013. [Online] [Accessed

[26] L. E. Murr and S. M. Gaytan, "10.06 - Electron Beam Melting A2," in *Comprehensive Materials Processing*, G. F. Batalha, C. J. V. Tyne, and B. Yilbas, Eds., ed Oxford: Elsevier, 2014, pp. 135-161.

[27] J. Karlsson, "Optimization of Electron Beam Melting for Production of Small Components in Biocompatible Titanium Grades," 2015.

[28] M. Y. P. Costa, H. J. C. Voorwald, W. L. Pigatin, V. A. Guimarães, and M. O. H. Cioffi, "Evaluation of shot peening on the fatigue strength of anodized Ti-6Al-4V alloy," *Materials Research,* vol. 9, pp. 107-109, 2006.

[29] Arcam AB, "Ti6Al4V ELI Titanium Alloy," n.d. [Online] Available: http://www.arcam.com/wp-content/uploads/Arcam-Ti6Al4V-ELI-Titanium-Alloy.pdf. [Accessed 28 April 2016].

[30] L. M. Gammon, R. D. Briggs, J. M. Packard, K. W. Batson, R. Boyer, and C. W. Domby, "Metallography and microstructures of titanium and its alloys," *Materials Park, OH: ASM International, 2004.,* pp. 899-917, 2004.

[31] B. Gaspar, "Microstructural characterization of Ti-6Al-4V and its relationship to sample geometry," 2012.

[32] H. K. Rafi, N. V. Karthik, H. Gong, T. L. Starr, and B. E. Stucker, "Microstructures and Mechanical Properties of Ti6Al4V Parts Fabricated by Selective Laser Melting and Electron Beam Melting," *Journal of Materials Engineering and Performance,* vol. 22, pp. 3872-3883, 2013.

[33] Allegheny Technologies Incorporated, "ATI 6-4 ELI (ATI Ti-6Al-4V-ELI, Grade 23)," 2011. [Online] Available: https://www.atimetals.com/Documents/ati_6-4eli_tds_en_v1.pdf. [Accessed 1 September 2016].

[34] Allegheny Technologies Incorporated, "ATI Ti-6Al-4V, Grade 5," 2011. [Online] Available: https://www.atimetals.com/Documents/ati_6-4_tds_en_v1.pdf. [Accessed 1 September 2016].

[35] ASTM F1108-14, Standard Specification for Titanium-6Aluminum-4Vanadium Alloy Castings for Surgical Implants (UNS R56406), ASTM International, West Conshohocken, PA, 2014,

[36] ASTM F1472-14, Standard Specification for Wrought Titanium-6Aluminum-4Vanadium Alloy for Surgical Implant Applications (UNS R56400), ASTM International, West Conshohocken, PA, 2014,

[37] M. Geetha, A. K. Singh, R. Asokamani, and A. K. Gogia, "Ti based biomaterials, the ultimate choice for orthopaedic implants - A review," *Progress in Materials Science,* vol. 54, pp. 397-425, May 2009.

[38] F. A. Shah, M. Trobos, P. Thomsen, and A. Palmquist, "Commercially pure titanium (cp-Ti) versus titanium alloy (Ti6Al4V) materials as bone anchored implants — Is one truly better than the other?," *Materials Science and Engineering: C,* vol. 62, pp. 960-966, 5/1/ 2016.

[39] F. A. Shah, A. Snis, A. Matic, P. Thomsen, and A. Palmquist, "3D printed Ti6Al4V implant surface promotes bone maturation and retains a higher density of less aged osteocytes at the bone-implant interface," *Acta Biomater,* vol. 30, pp. 357-67, Jan 15 2016.

[40] J. Robertson, "Diamond-like amorphous carbon," *Materials Science & Engineering R-Reports,* vol. 37, pp. 129-281, May 24 2002.

[41] A. Grill, "Diamond-like carbon: state of the art," *Diamond and Related Materials,* vol. 8, pp. 428-434, 3// 1999.

[42] D. H. Kim, H. E. Kim, K. R. Lee, C. N. Whang, and I. S. Lee, "Characterization of diamond-like carbon films deposited on commercially pure Ti and Ti-6Al-4V," *Materials Science & Engineering C-Biomimetic and Supramolecular Systems,* vol. 22, pp. 9-14, Oct 1 2002.

[43] A. Boogaard, "Plasma-enhanced chemical vapor deposition of silicon dioxide: optimizing dielectric films through plasma characterization," 2011.

[44] J. A. Bottomley, "Novel application of atomic force microscopy to the analysis of barrier film defects," University of Birmingham, 2012.

[45] W. Bauer, M. Weber, and S. Chanbai, "White Light Interferometry," in *Encyclopedia of Tribology*, Q. J. Wang and Y.-W. Chung, Eds., ed Boston, MA: Springer US, 2013, pp. 4115-4127.

[46] Materials Evaluation and Engineering Incorporated, "Energy Dispersive X-Ray Spectroscopy (EDS)," n.d. [Online] Available: http://www.mee-inc.com/hamm/energy-dispersive-x-ray-spectroscopyeds/. [Accessed 9 September 2016].

[47] The University of California, "Introduction to Energy Dispersive X-ray Spectrometry (EDS)," n.d. [Online] Available: http://cfamm.ucr.edu/documents/eds-intro.pdf. [Accessed 12 October 2016].

[48] Thermo Fisher Scientific Incorporated, "What is X-Ray Photoelectron Spectroscopy (XPS)?," n.d. [Online] Available: http://xpssimplified.com/whatisxps.php. [Accessed 1 September 2016].

[49] S. Axelsson, "Surface Characterization of Titanium Powders with X-ray Photoelectron Spectroscopy," CHALMERS UNIVERSITY OF TECHNOLOGY Gothenburg, Sweden, 2012.

[50] Thermo Fisher Scientific Incorporated, "Ion Scattering Spectroscopy," n.d. [Online] Available: http://xpssimplified.com/ion_scattering_spectroscopy.php. [Accessed 1 September 2016].

[51] P. P. Ackermans, "Surface analysis by low-energy ion scattering: two-dimensional detection and quantification," Technische Universiteit Eindhoven, 1990.

[52] W. Abdallah, J. S. Buckley, A. Carnegie, J. Edwards, B. Herold, E. Fordham, *et al.*, "Fundamentals of wettability," *Technology,* vol. 38, p. 268, 1986.

[53] Y. Yuan and T. R. Lee, "Contact angle and wetting properties," in *Surface science techniques*, ed: Springer, 2013, pp. 3-34.

[54] National Institute of Biomedical Imaging and Bioengineering, "Tissue Engineering and Regenerative Medicine," n.d. [Online] Available: https://www.nibib.nih.gov/science-education/science-topics/tissue-engineering-and-regenerative-medicine. [Accessed 29 August 2016].

[55] Y. Luo, G. Engelmayr, D. T. Auguste, L. da Silva Ferreira, J. M. Karp, R. Saigal, *et al.*, "Chapter 24 - 3D Scaffolds," in *Principles of Tissue Engineering (Fourth Edition)*, ed Boston: Academic Press, 2014, pp. 475-494.

[56] H. N. Chia and B. M. Wu, "Recent advances in 3D printing of biomaterials," *J Biol Eng,* vol. 9, p. 4, 2015.

[57] G. Binyamin, B. M. Shafi, and C. M. Mery, "Biomaterials: a primer for surgeons," *Semin Pediatr Surg,* vol. 15, pp. 276-83, Nov 2006.

[58] M. Navarro, A. Michiardi, O. Castaño, and J. A. Planell, "Biomaterials in orthopaedics," *Journal of the Royal Society Interface,* vol. 5, pp. 1137-1158, 2008.

[59] C. Pautke, M. Schieker, T. Tischer, A. Kolk, P. Neth, W. Mutschler*, et al.*, "Characterization of osteosarcoma cell lines MG-63, Saos-2 and U-2 OS in comparison to human osteoblasts," *Anticancer research,* vol. 24, pp. 3743-3748, 2004.

[60] M. Prideaux, A. R. Wijenayaka, D. D. Kumarasinghe, R. T. Ormsby, A. Evdokiou, D. M. Findlay*, et al.*, "SaOS2 Osteosarcoma Cells as an In Vitro Model for Studying the Transition of Human Osteoblasts to Osteocytes," *Calcified Tissue International,* vol. 95, pp. 183-193, Aug 2014.

[61] S. Adam Hacking and A. Khademhosseini, "Chapter II.1.3 - Cells and Surfaces in vitro A2 - Ratner, Buddy D," in *Biomaterials Science (Third Edition)*, A. S. Hoffman, F. J. Schoen, and J. E. Lemons, Eds., ed: Academic Press, 2013, pp. 408-427.

[62] C. M. Nelson and C. S. Chen, "Engineering cell adhesion for applications in biotechnology."

[63] H. Schatten, "Mitosis A2 - Maloy, Stanley," in *Brenner's Encyclopedia of Genetics (Second Edition)*, K. Hughes, Ed., ed San Diego: Academic Press, 2013, pp. 448-451.

[64] National Institute of Arthritis and Musculoskeletal and Skin Diseases, "Scientists Gain New Clues to Bone Mineralization," 2006. [Online] Available: http://www.niams.nih.gov/news_and_events/spotlight_on_research/2006/bone_mineralization.asp. [Accessed 9 August 2016].

[65] M. I. Jamaludin, N. A. A. Kasim, N. H. M. Nor, and M. H. Ismail, "Development of Porous Ti-6Al-4V Mix with Palm Stearin Binder by Metal Injection Molding Technique," *American Journal of Applied Sciences,* vol. 12, p. 742, 2015.

[66] R. Li, L. Riester, T. R. Watkins, P. J. Blau, and A. J. Shih, "Metallurgical analysis and nanoindentation characterization of Ti–6Al–4V workpiece and chips in high-throughput drilling," *Materials Science and Engineering: A,* vol. 472, pp. 115-124, 2008.

[67] Y. Kok, X. Tan, S. B. Tor, and C. K. Chua, "Fabrication and microstructural characterisation of additive manufactured Ti-6Al-4V parts by electron beam melting: This paper reports that the microstructure and micro-hardness of an EMB part is thickness dependent," *Virtual and Physical Prototyping,* vol. 10, pp. 13-21, 2015.

[68] R. Klingvall Ek, R. Klingvall Ek, L.-E. Rännar, L.-E. Rännar, M. Bäckstöm, M. Bäckstöm*, et al.*, "The effect of EBM process parameters upon surface roughness," *Rapid Prototyping Journal,* vol. 22, pp. 495-503, 2016.

[69] A. Safdar, H. He, L.-Y. Wei, A. Snis, and L. E. Chavez de Paz, "Effect of process parameters settings and thickness on surface roughness of EBM produced Ti-6Al-4V," *Rapid Prototyping Journal,* vol. 18, pp. 401-408, 2012.

[70] M. Ask, J. Lausmaa, and B. Kasemo, "Preparation and surface spectroscopic characterization of oxide films on Ti6Al4V," *Applied Surface Science,* vol. 35, pp. 283-301, 1989/01/01 1989.

[71] J. Vaithilingam, E. Prina, R. D. Goodridge, R. J. M. Hague, S. Edmondson, F. R. A. J. Rose, *et al.*, "Surface chemistry of Ti6Al4V components fabricated using selective laser melting for biomedical applications," *Materials Science and Engineering: C,* vol. 67, pp. 294-303, 10/1/ 2016.

[72] S. Ponader, E. Vairaktaris, P. Heinl, C. v. Wilmowsky, A. Rottmair, C. Körner, *et al.*, "Effects of topographical surface modifications of electron beam melted Ti-6Al-4V titanium on human fetal osteoblasts," *Journal of biomedical materials research Part A,* vol. 84, pp. 1111-1119, 2008.

Appendices

Appendix A: Consultation Meetings Attendance Form

Consultation Meetings Attendance Form

Week	Date	Comments (if applicable)	Student's Signature	Supervisor's Signature
1	1/8/16	· Project Plan and Introduction · In Person		
2	15/8/16	· Weekly update of project. · Email		
3	23/8/16	· Weekly update of project. · Email		
4	30/8/16	· Weekly update of project. · Email		
5	5/9/16	· Weekly update of project. · Email		
6	14/9/16	· Weekly update of project. · Email		
7	23/9/16	· Discussed Feedback from progress report. · In Person		
8	9/10/16	· Discussed presentation of results. · In Person		
9	13/10/16	· Discussed presentation and discussion section of report. · In Person		
10	20/10/16	· Weekly update of project · In Person		
11	1/11/16	· Review of draft thesis · Email		
12	3/11/16	· Review of draft thesis · Email		

Appendix Figure 1 Consultation Meetings Attendance Form